

Alloy Nanoparticles for Hydrogen Sensing

A study of hydrogen sorption properties in gold-palladium nanoparticles

Master thesis in Master Programme Nanotechnology

SUNE LEVIN

MASTER THESIS 2016

Alloy Nanoparticles for Hydrogen Sensing

A study of hydrogen sorption properties in gold-palladium nanoparticles

Master thesis in Master Programme Nanotechnology

SUNE LEVIN



Department of Physics
Division of Chemical physics
Nanoplasmonics
CHALMERS UNIVERSITY OF TECHNOLOGY
Gothenburg, Sweden 2016

Alloy Nanoparticles for Hydrogen Sensing
A study of hydrogen sorption properties in gold-palladium nanoparticles
SUNE LEVIN

© SUNE LEVIN, 2016.

Supervisor: Ferry Nugroho, PhD Student, Chemical Physics, Department of Physics
Examiner: Christoph Langhammer, Associate Professor, Chemical Physics, Department of Physics

Master Thesis 2016:NN
Department of Physics
Division of Chemical Physics
Nanoplasmonics
Chalmers University of Technology
SE-412 96 Gothenburg
Telephone +46 31 772 1000

Cover: Hydrogen sorption isotherms in PdAu alloy nanoparticles containing 10% gold. Here in combination with illustrations of nanoparticles to clarify how the isotherm curves display the absorption and desorption of hydrogen.

Typeset in L^AT_EX
Gothenburg, Sweden 2016

Alloy Nanoparticles for Hydrogen Sensing
A study of hydrogen sorption properties in gold-palladium nanoparticles
SUNE LEVIN
Department of Physics
Chalmers University of Technology

Abstract

Detecting hydrogen with nanoplasmonic sensing is a fairly new concept with the promising prospect of producing compact and precise hydrogen sensors with a low cost, due to the small amount of materials needed. In order to explore this possibility, material properties of various nanoparticle compositions should be examined to get a good understanding for these systems as well as finding the most suitable materials. In this master thesis project I have studied absorption and desorption of hydrogen in PdAu alloy nanoparticles to determine their thermodynamic and kinetic properties. This was done with direct nanoplasmonic sensing utilizing the change in LSPR (Localized Surface Plasmon Resonance) when changing the concentration of hydrogen in the nanoparticles. The main focus has been on determining the critical temperature T_C for PdAu alloy nanoparticles with a concentration of gold ranging from 0 to 30 at%. Using two different methods, Van't Hoff equation and data collapse, T_C is found to decrease with increasing gold concentration. This decrease goes from $\sim 250^\circ\text{C}$ for pure palladium to below 100°C for alloys with gold concentration greater than 15 at%. For gold concentrations of 20% and above, T_C might already be below room temperature, but an unexpected hysteresis present at all hydrogen pressures was found, complicating the result interpretation. The reason behind this hysteresis is widely discussed in this report and the most likely explanation seems to be particle-substrate strain. Furthermore, the response time of the rate limiting step t_{90} for both hydrogen absorption and desorption is found to decrease with increased gold concentration. A quantitative description of the energy landscape for hydrogen desorption was also derived by continuously analyzing change in the LSPR signal of the alloy particles during dehydrogenation.

Keywords: Alloy nanoparticles, hydrogen sensing, nanoplasmonics, LSPR, PdAu, HCL, critical temperature, response time, energy landscape.

Acknowledgements

I thank Ferry Nugroho for being an excellent supervisor who is always cheerful and available for advice. I thank Christoph Langhammer for being an inspirational examiner with original ideas and great ways of explaining anything I might dwell on. I thank my family and friends for always being there to support me as well as my great colleagues at chemical physics.

This thesis could not have been done without you.

Sune Levin, Gothenburg, August 16, 2016

Contents

List of Figures	xi
List of Tables	xv
1 Introduction	1
1.1 Background	1
1.2 Purpose	2
1.3 Scope	2
2 Theory	3
2.1 Plasmonic nanoparticles	3
2.1.1 Localized surface plasmon resonance	3
2.1.2 Sensing using plasmonic nanoparticles	5
2.2 Hydrogen storage in metals	5
2.2.1 Ways to diminish the hysteresis	6
2.2.2 Van't Hoff equation	7
2.2.3 Determining critical temperature with data collapse	7
2.3 Geometry of two layer deposition for alloy nanoparticles	8
3 Experimental methods and HCL fabrication	11
3.1 Alloy nanoparticle array fabrication	11
3.2 Hydrogen sorption measurement setup	14
3.3 Experimental procedure	14
4 Results and discussion	15
4.1 Energetics	15
4.1.1 Critical temperature	19
4.2 Kinetics	23
4.2.1 Energy landscape	24
4.3 Relation between extinction spectrum descriptors	25
5 Conclusions	27
5.1 Outlook	28
Bibliography	29
A Appendix 1	I

Contents

A.1	HCL alloy fabrication details	I
A.2	Additional isotherms	I
A.3	More relations between extinction spectrum descriptors	IV
A.4	Van't Hoff plots	X
A.5	Data collapse for S1	XIII

List of Figures

2.1	The images show (a) how the electron cloud for a nanoparticle oscillates by interaction with the electric field from light. (b) a locally enhanced electric field caused by the oscillating electron cloud. (c) higher modes in which the electron cloud of larger nanoparticles (in relation to wavelength) can oscillate.	4
2.2	Left we see a typical extinction spectrum from a plasmonic nanoparticle (Au in this case) and how the different values of extinction, peak position and FWHM are evaluated from the spectrum. To the right the spectrum from Pd is compared to a extinction spectrum from hydrogenated Pd nanoparticles to show how the change in extinction spectrum results in shifts in peak position and extinction.	5
2.3	The left image shows how hydrogen distributes itself in the metal lattice depending on the hydrogen to metal concentration going from α to β -phase. The energy difference of the two phases are created by lattice strain and gives rise to the typical hysteresis of hydrogen sorption in palladium seen in the graph to the right. Here we also see a slight slope of the plateau commonly seen for Pd nanoparticles. This slope is probably caused by slightly varying plateau pressure for different absorption sites in the nanoparticles caused by substrate-particle strain [16], as well as by particle-specific plateau pressures of the nanoparticles in the measured ensemble [17].	6
2.4	The graph shows the calculated atomic percentage of Ag and Au in PdAg and PdAu disks as a function of layer height when first depositing Ag or Au and then Pd. We see that the curves are nearly identical due to Ag and Au having close to the same volumetric density.	9
3.1	(a) Clean substrate. (b) Spin-coated with PMMA. (c) Drip coated with PDDA. (d) Drip coated with PS beads. (e) Evaporation of Cr. (f) Removing PS beads with tape stripping. (g) Oxygen plasma etching. (h) Leaving a holmask ready for deposition of metals to form nanoparticles. The figure is adapted with kind permission from [23]. .	12

3.2	(a,b,c) Successive deposition of metals. (d) Lift-off using acetone leaving the substrate with only the metal nanoparticles. (e) An illustration of how a metal layer nanoparticle disk looks after evaporating metals but before annealing it into an alloy. In this thesis, this process was only performed with two layers but the principle is exactly the same. The figure is adapted with kind permission from [23].	12
3.3	The experimental setup for measuring hydrogen sorption is illustrated here. The sample is put into a vacuum chamber where hydrogen gas pressure is controlled and monitored by valves and pressure meters. Light is shone through the sample and compared with a reference signal to get the extinction spectrum and the temperature is kept constant by a thermocouple. The measured values are then transferred to a computer collecting the data.	13
4.1	The figure shows the first measurement series (S1) of isotherms for PdAu nanoparticles with varying amount of gold, 0, 10, 20 and 30%, and at different temperatures. As the temperature rises the hysteresis decreases and for higher concentrations of gold there is nearly no hysteresis already at room temperature. Here the extinction at peak position is showing how much hydrogen is absorbed. For the same series but with relative peak position, see appendix A.2.	17
4.2	The figure shows the second measurement series (S2) of isotherms for PdAu nanoparticles with varying amount of gold, 5, 10, 15, 20, 25 and 30%, and at different temperatures. The general shapes of the isotherms are very similar to S1 indicating reproducibility. The measurements at 25% gold are a bit out of the trend and show a more prominent hysteresis at phase transition. Further research should look into if this is simply happenstance or if this may be some phenomenon related to crystal structure. Also here the extinction at peak position is showing how much hydrogen is absorbed. For the same series but with relative peak position, see appendix A.2. For the measurement of 0% gold in this series see figure A.3	18
4.3	A typical Van't Hoff plot showing how the gap between enthalpy of absorption and desorption decreases until the critical temperature is reached. In this particular example it is used to calculate the critical temperature of pure Pd nanoparticles, giving a value of 197.4°C. Additional Van't Hoff plots used in this thesis are found in appendix A.4.	19
4.4	Two different ways to determine the critical temperature with either Van't Hoff analysis or the simplest lattice gas model with linear H-H interactions is shown above. The comparison demonstrates how the linear approximation of the Van't Hoff equation underestimates the critical temperature for measurements far away from T_C . The figure is adapted from reference [21].	20

4.5	To the left we see the critical temperatures of a series of PdAu nanoparticles calculated with data collapse, assuming the spinodal fits will scale with the same k-factor. To the right the same values are shown but to the scale of the absolute temperature instead of the temperature relative to individual T_C . These graphs display the analysis for S2. However, data collapse was also done on S1, shown in appendix A.5.	22
4.6	The graph shows a summary of calculated critical temperatures with the values seen in Table 4.1. A general trend is seen with T_C decreasing from slightly above 200°C down to around 100 °C. The Van't Hoff method on S2 shows a low value for 0% gold, probably due to only using temperatures up to 100°C resulting in an underestimation from the linear approximation of the method far from T_C	22
4.7	Both graphs show the normalized extinction when absorbing (to the left) or desorbing (to the right) hydrogen, going from vacuum to 1 bar or from 1 bar to vacuum. The increase in speed with increased gold concentration is very clear as well as the fact that the desorption process is slower than the absorption process.	23
4.8	A summary of the response time for PdAu nanoparticles of varying gold concentration is seen in the graph above. The trend of increasingly faster kinetics with higher gold concentration is clear. However, the value at 20% gold is deviating from the trend.	24
4.9	A series of graphs displaying the energy landscape of the evolution of the activation barrier for associative H_2 desorption from the surface for samples with increasing the gold concentration. The energy increases for the first few steps of increase in gold concentration, but then decreases steadily.	25
4.10	The graphs compare the two descriptors, peak position and extinction at peak position for the measurements at 30°C presented in figure 4.2. This kind of comparisons can be done with FWHM as well and may also be done at all temperatures, see appendix A.3. The information stored in this data may very well provide for better understanding of the plasmonics of metal hydride alloy nanoparticles.	26
A.1	The figure shows the second measurement series (S2) of isotherms for PdAu nanoparticles with varying amount of gold, 5, 10, 15, 20, 25 and 30%, and at different temperatures, but extracted from peak position instead of extinction. Also here, both ways of interpreting the data show the same trends but with slight variation in shape. For 0% gold see figure A.3	II
A.2	The figure shows the first measurement series (S1) of isotherms for PdAu nanoparticles with varying amount of gold, 0, 10, 20 and 30%, and at different temperatures, but extracted from peak position instead of extinction. Both ways to interpret the data show the same trends but with slight variation in shape.	III

A.3	The figure show isotherms from S2 for 0% gold concentration extracted from extinction at peak position to the left and from peak position to the right. The general shapes are very similar to those of S1 for 0% seen in figure 4.1 and A.2, indicating reproducibility.	III
A.4	The graphs compare peak position with the extinction at peak position for the measurements at 40°C presented in figure 4.2.	IV
A.5	The graphs compare peak position with the extinction at peak position for the measurements at 50°C presented in figure 4.2.	V
A.6	The graphs compare peak position with the extinction at peak position for the measurements at 60°C presented in figure 4.2.	V
A.7	The graphs compare peak position with the extinction at peak position for the measurements at 80°C presented in figure 4.2.	VI
A.8	The graphs compare peak position with the extinction at peak position for the measurements at 100°C presented in figure 4.2.	VI
A.9	The graphs compare FWHM with the extinction at peak position for the measurements at 30°C presented in figure 4.2.	VII
A.10	The graphs compare FWHM with the extinction at peak position for the measurements at 40°C presented in figure 4.2.	VII
A.11	The graphs compare FWHM with the extinction at peak position for the measurements at 50°C presented in figure 4.2.	VIII
A.12	The graphs compare FWHM with the extinction at peak position for the measurements at 60°C presented in figure 4.2.	VIII
A.13	The graphs compare FWHM with the extinction at peak position for the measurements at 80°C presented in figure 4.2.	IX
A.14	The graphs compare FWHM with the extinction at peak position for the measurements at 100°C presented in figure 4.2.	IX
A.15	The graphs compare peak position with the extinction at peak position for the measurements at 30°C done by Ferry Nugroho. We here see very similar trends to the ones in figure 4.10, however with a more pronounced hysteresis due to shorter annealing time.	X
A.16	The graph shows the Van't Hoff plot for evaluating T_C for 10% gold in measurement series S1.	XI
A.17	The graph shows the Van't Hoff plot for evaluating T_C for 0% gold in measurement series S2.	XI
A.18	The graph shows the Van't Hoff plot for evaluating T_C for 5% gold in measurement series S2.	XII
A.19	The graph shows the Van't Hoff plot for evaluating T_C for 10% gold in measurement series S2.	XII
A.20	The graph shows the Van't Hoff plot for evaluating T_C for 15% gold in measurement series S2.	XIII
A.21	In this graph data collapse on S1 is shown. The amount of contribution from isotherms with large overall hysteresis gives a fairly low k -factor of 0.526. This contribution most likely results in a slight overestimation of T_C	XIII

List of Tables

4.1	The table shows critical temperature values from the two different methods of calculating T_C . The value calculated with Van't Hoff analysis for 15% gold diverts from the trend, probably due to the large overall hysteresis in comparison with the normal hysteresis. The squares without values are not possible to calculate with Van't Hoff's equation due to the overall hysteresis.	21
4.2	Energetics for PdAu of different alloy concentrations calculated with Van't Hoff analysis. Values for higher gold concentrations were not possible to calculate due to the increasing overall hysteresis.	23

1

Introduction

The possibility to replace fossil fuel in favor of hydrogen has many benefits in that it can be made fully renewable and leaves only water as waste [1]. However, the prospect of using hydrogen as main energy carrier still has many tasks to solve, such as its compact storage and efficient production. Safety is another issue, since hydrogen is known for its high flammability when mixed with air (4-75 vol. %).

With the introduction of hydrogen fuel cell cars on the market only a few years ago, a rising need for fast and accurate hydrogen sensors can be anticipated. To answer these needs, new sensor techniques such as nanoplasmonic alloy hydrogen sensors [2] are being developed. In this thesis I will go into detail on how plasmonic alloy nanoparticles can be used in hydrogen sensing and the different properties observed when the alloy composition is varied.

1.1 Background

During the last year a method of constructing arrays of supported alloy nanoparticles, with remarkably high precision in alloy composition has been established [3]. This allows for a wide field of experiments to be made to explore the physics and chemistry of such systems. Taking advantage of this new technique, I have fabricated samples of Palladium-Gold (PdAu) alloy nanoparticles and studied their hydrogen sorption properties. This has been done to get a better understanding of how hydrogenation occurs in alloy nanoparticles which in turn will help creating the foundation for a fast and sensitive hydrogen sensing technique.

By using plasmonic nanoparticles the hydrogen concentration in the particles can be determined by measuring their extinction spectra. This technique, monitoring changes directly in the plasmonic material, is called *direct nanoplasmonic sensing*. With additional research and optimization, this technique has the possibility of providing incredibly compact, cheap and efficient hydrogen sensors. This is because of the low amount of materials needed to create the device and the sensing can be done with a low cost LED lamp for an optimized system. However, to achieve such sensors, the properties of alloy nanoparticles need to be determined and understood in order for us to be able to engineer the material properties to our advantage. The properties measured and discussed here will be enthalpy, entropy, response time and energy of both absorption and desorption as well as critical temperature.

The critical temperature T_C is a highly important property when hydrogen sensing is concerned. T_C is when a transition between two phases α and β in hydrogen sorption occur continuously. When this transition does not occur continuously a hysteresis is

formed, causing the amount of hydrogen to not only depend on hydrogen pressure around the particle but also on whether that pressure is increasing or decreasing. Such hysteresis is an inherent property of most of hydride-forming metal and is also found in Pd. This is undesirable for sensing purposes since different input pressure can result in the same output from the sensor and vice versa. For bulk palladium the T_C is known to be $\sim 300^\circ\text{C}$ [4, 5] and it decreases slightly when going to thin film or nanoparticles. I will in this thesis show that it decreases even more for PdAu alloys. With no prior studies made on PdAu alloy nanoparticles this work is breaking new grounds in terms of determining critical temperature for such nanostructures.

1.2 Purpose

In this master's thesis I aim to explore hydrogen sorption properties in PdAu alloy nanoparticles fabricated by a recently established method [3]. The critical temperatures as well as energetic and kinetics properties are determined for alloy concentrations ranging from 0 to 30 at% of Au. This is done to explore the physics of hydrogen absorption and desorption in nanoparticle alloys and in this way contribute to the fields of hydrogen sensing and nanoplasmonic sensing.

1.3 Scope

The study covers determination of kinetics and energetic properties of gold-palladium nanoparticles disks of size 190 nm x 25 nm with varying alloy compositions. Alloy nanoparticle array samples were prepared in the cleanroom of Chalmers and various measuring techniques were used to determine sought properties. Along with the fabrication and experimental measurements, a substantial amount of data analysis was performed in MATLAB to evaluate experimental data. This data evaluation regards two different ways to determine critical temperatures for PdAu nanoparticles that were explored and discussed to narrow down how to qualitatively define critical temperature for Pd alloy nanoparticles. Furthermore, response times and energy landscapes for hydrogen absorption and desorption have been extracted from kinetic measurements.

2

Theory

Using alloy nanoparticles for hydrogen sensing is based on a few different properties of metal nanoparticles. To get a full understanding of the concept I will in this chapter go through these properties, specifically the hydrogen storage in metals and nanoparticle plasmonics. I will then explain what happens when going to alloy nanoparticles from pure metal nanoparticles and why this is needed for hydrogen sensing.

2.1 Plasmonic nanoparticles

Even though the interesting properties of metal nanoparticles have been utilized for centuries in light absorption and scattering, for example in stained glass decorating many churches, the field of nanoplasmonics did not pick up speed until about two decades back [6]. In this field one utilizes the distinct way of which noble metal nanoparticles interact with light for purposes such as increased light absorption [7], targeted radiation cancer treatment [8,9] and sensing [2,3]. To follow how I have used this phenomenon for hydrogen sensing I will now go through the basics of plasmon oscillations caused by particle-light interaction.

2.1.1 Localized surface plasmon resonance

When metal nanoparticles reach a size smaller than the wavelength of light its optical properties change. At this size the electric field from the light on the particle will drive an oscillation of the particles electron cloud, see figure 2.1. This oscillation is called LSPR (Localized Surface Plasmon Resonance) and its energy (frequency) varies with particle size, shape, dielectric function and the dielectric constant of surrounding media [10]. Since energy is taken from the electric field, light is effectively absorbed and scattered due to these oscillations.

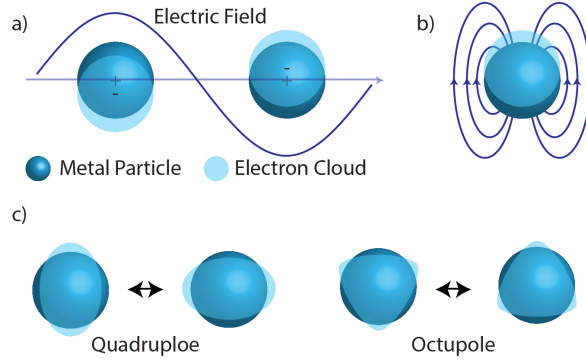


Figure 2.1: The images show (a) how the electron cloud for a nanoparticle oscillates by interaction with the electric field from light. (b) a locally enhanced electric field caused by the oscillating electron cloud. (c) higher modes in which the electron cloud of larger nanoparticles (in relation to wavelength) can oscillate.

The resonance can be approximated by assuming a spherical nanoparticle with diameter $D \ll \lambda$, where λ is the light wavelength. With this assumption, the dipole moment \mathbf{P} from the electric field can be described as

$$\mathbf{P}(\omega) = \epsilon_d \alpha(\omega) \mathbf{E}_0 e^{-i\omega t}, \quad (2.1)$$

where ϵ_d is the dielectric constant of surrounding media, $\alpha(\omega)$ is the dipole polarizability of the nanoparticle and $\mathbf{E}_0 e^{-i\omega t}$ is the electric field. From Mie theory [11] the polarizability can be written as

$$\alpha(\omega) = 4\pi \left(\frac{D}{2}\right)^3 \frac{\epsilon_p(\omega) - \epsilon_d}{\epsilon_p(\omega) + 2\epsilon_d}, \quad (2.2)$$

where $\epsilon_p(\omega)$ is the complex dielectric function of the nanoparticle material. This expression can be approximated as

$$\alpha(\omega) \approx 4\pi \left(\frac{D}{2}\right)^3 \frac{\omega_{LSPR}^2}{\omega_{LSPR}^2 - \omega^2 - i\Gamma\omega}, \quad (2.3)$$

where $\omega_{LSPR} = \frac{\omega_p}{\sqrt{1+2\epsilon_d}}$ is the LSPR-frequency. This is done by assuming the Drude dielectric function $\epsilon_p(\omega) = 1 - \frac{\omega_p^2}{\omega^2 - i\Gamma\omega}$. This assumption models the electrons as an ideal Fermi gas and assumes no electron-electron interaction and weak electrostatic field in the metal due to screening effects [12]. From ω_{LSPR} we can get the LSPR-wavelength

$$\lambda_{LSPR} = \lambda_p \sqrt{1 + 2\epsilon_d}, \quad (2.4)$$

where the most light is scattered and absorbed due to the plasmon oscillations. Effectively this means that the extinction spectrum from light consumed by absorption and scattering will peak at this particular wavelength.

2.1.2 Sensing using plasmonic nanoparticles

By just looking at equation (2.4), we see that λ_{LSPR} depends on λ_P determined by properties of the nanoparticle and ϵ_d determined by surrounding media. Therefore, changes in either nanoparticle properties (for example amount of reactants on the surface in a catalytic reaction or hydrogen concentration) or dielectric of surrounding media can be probed by measuring changes in the LSPR-wavelength peak. Prior research [2,3] has shown that hydrogen sorption in PdAu nanoparticles can be characterized with this technique.

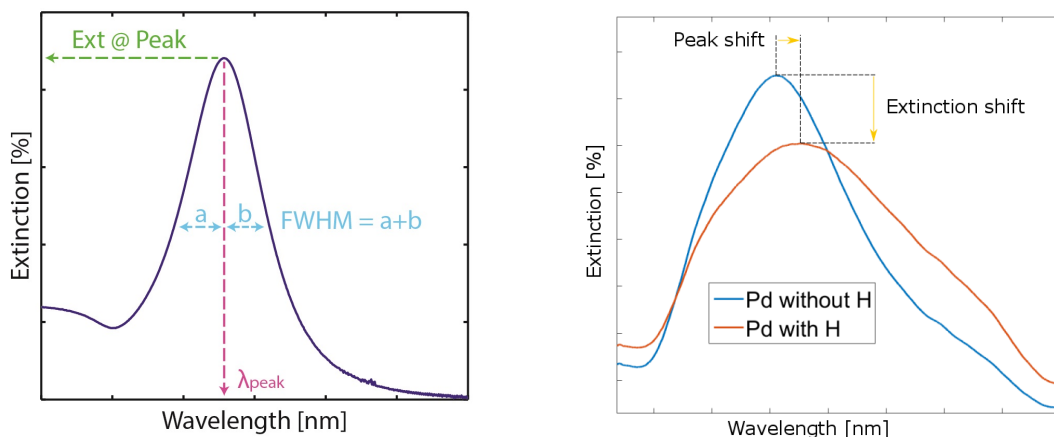


Figure 2.2: Left we see a typical extinction spectrum from a plasmonic nanoparticle (Au in this case) and how the different values of extinction, peak position and FWHM are evaluated from the spectrum. To the right the spectrum from Pd is compared to a extinction spectrum from hydrogenated Pd nanoparticles to show how the change in extinction spectrum results in shifts in peak position and extinction.

Other than monitoring the LSPR-peak, the extinction at peak position as well as the FWHM (Full Width Half Maximum) of the peak may be used to observe the hydrogen absorption. This is presented in figure 2.2 where these different quantities are illustrated in comparison to the extinction spectrum. While the peak position correlates linearly to the hydrogen percentage in Pd nanoparticles [13], the other descriptors do not follow the peak position exactly. However, they follow close enough to give a good approximation of the hydrogen concentration and the small differences may very well contain additional information of the hydrogenation process. In this thesis I am mainly presenting results from the extinction at peak position since this gives by far the best signal to noise ratio.

2.2 Hydrogen storage in metals

The fact that hydrogen diffuses into metals, particularly in palladium, in which it occurs spontaneously, was discovered already about 150 years ago by Thomas Graham [14]. Due to the very small size of the hydrogen atoms, they sit in between the atoms of a metal lattice (i.e. interstitial sites). This works particularly well in

palladium which has the property of dissociating hydrogen molecules even at room temperature and can store up to 900 times its volume of hydrogen [15].

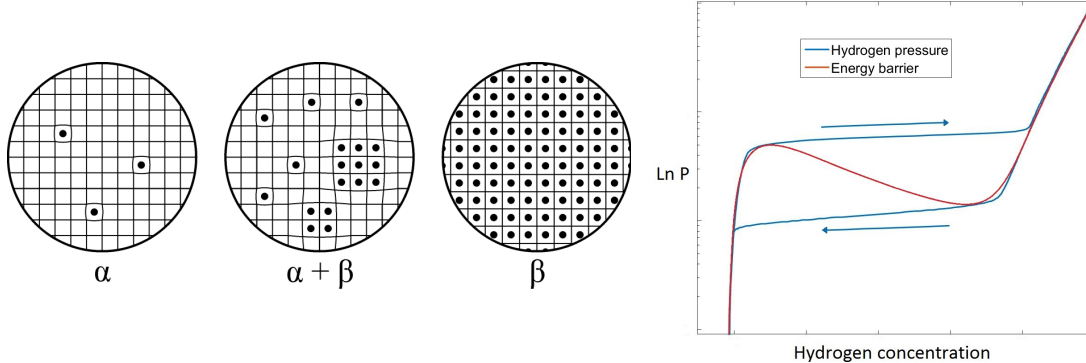


Figure 2.3: The left image shows how hydrogen distributes itself in the metal lattice depending on the hydrogen to metal concentration going from α to β -phase. The energy difference of the two phases are created by lattice strain and gives rise to the typical hysteresis of hydrogen sorption in palladium seen in the graph to the right. Here we also see a slight slope of the plateau commonly seen for Pd nanoparticles. This slope is probably caused by slightly varying plateau pressure for different absorption sites in the nanoparticles caused by substrate-particle strain [16], as well as by particle-specific plateau pressures of the nanoparticles in the measured ensemble [17].

When absorbing hydrogen the metal lattice is strained in a way described by figure 2.3. As the amount of hydrogen increases, the metal goes from a pure metallic state α to a mixed state $\alpha + \beta$ and ends up in a metal hydride state β [18, 19]. From figure 2.3 showing an isotherm measurement of Pd nanoparticles, we can see how the difference in strain between these states create an energetic difference between absorption and desorption. This energy difference makes it favourable to absorb most of the hydrogen at a certain pressure and desorb hydrogen at another pressure, forming a hysteresis with two different pressures where the phase transition occurs. Such hysteresis is undesirable for sensor applications, since it will give different results depending on whether the hydrogen concentration is increasing or decreasing. However, one can also utilize the plateaus to read out the plateau pressures at which the phase transition occurs. By doing this for several isotherms at different temperatures, energetic properties and T_C can be determined from the plateau pressures. Furthermore, the hysteresis can be diminished by going to higher temperatures (i.e. above T_C) or creating an alloy together with another metal which I will now discuss in more detail.

2.2.1 Ways to diminish the hysteresis

The temperature required for the hysteresis in hydrogen sorption to disappear is called the critical temperature T_C . At this temperature the energy no longer decreases when going from one phase to another making the transition continuous.

This effectively removes the hysteresis and gives a more linear relation between hydrogen pressure and concentration which is preferable for sensing applications. It has been shown that one way to decrease T_C is to decrease the nanoparticle size. This is due to the high percentage of surface in the particle and a large curvature which increases the particles surface energy. The higher surface energy gives rise additional compressive lattice strain when increasing hydrogen concentration which increases the change in enthalpy when going from α to β phase. This gives a higher energy of the β phase and thereby reduces the energy difference [19]. Another way to strain the Pd lattice is to add a metal of larger atom size such as gold, used in this thesis. This pre-strains the lattice, widening it and gives "more room" for the hydrogen atoms which results in a reduction of the energy difference between the two phases. This has been done in practice before by Wadell et al. [2]. With this approach the hysteresis disappear at room temperature while the signal strength (the size of the shift in extinction spectrum) is kept high through the highly-sensitive nature of the used plasmonic sensing method.

2.2.2 Van't Hoff equation

The Van't Hoff equation describes how changes in the equilibrium constant K_{eq} of a chemical reaction relates to the change in enthalpy ΔH and entropy ΔS at a given temperature T . It was suggested by Jacobus Henricus Van't Hoff in 1884 [20] and has since been commonly used to describe the changes of thermodynamic systems. In its linear form the equation is written as

$$\ln(K_{eq}) = -\frac{\Delta H}{RT} + \frac{\Delta S}{R}, \quad (2.5)$$

where R is the ideal gas constant. Hence by extracting values of $\ln(K_{eq})$ at different temperatures and fitting those to a linear curve, one can determine the change in both enthalpy and entropy of a given reaction. This is straightforward for hydrogen sorption isotherms since the equilibrium constant is given by the plateau pressure. Since one line is given from both absorption and desorption finding the intersection between these two lines gives the critical temperature where the hysteresis disappears. This is however not entirely true since the linear approximation is not exact, especially far away from the critical temperature [21]. Because of this inaccuracy, I have in this work also used an alternative way to calculate critical temperatures for palladium nanoparticles. By comparing the result from two different methods I hope to add more "meat to the bone" for discussion on how to determine critical temperatures for metal and alloy nanoparticles.

2.2.3 Determining critical temperature with data collapse

Another way to find the critical temperature for Pd nanoparticles was recently presented by Griessen et al. [21]. He notes that due to a slope in the phase transition plateaus of hydrogen sorption in nanoparticles it is hard to accurately determine the plateau pressure. However, the gap between the different plateaus is often close to constant which makes it reasonable to use the width of the gap, as it is better defined,

instead of the plateau pressure. By assuming a linear effective H-H interaction in the metal lattice Griessen derived the following formula for the hysteresis width

$$f(k, \frac{T_C}{T}) = k \cdot \left[8 \cdot \frac{T_C}{T} \sqrt{1 - \frac{T}{T_C}} + 4 \cdot \ln \left(\frac{1 - \sqrt{1 - \frac{T}{T_C}}}{1 + \sqrt{1 - \frac{T}{T_C}}} \right) \right],$$

where f is the hysteresis gap height, T_C is the critical temperature, T is the temperature of the measurement and k is a scaling factor. Since this formula only depends on the scaled temperature T_C/T it is possible to collapse data from several measurements on the same curve to find the optimal value for k . The curves fitted with the optimal k then give the critical temperatures since all of them already have their own value for T_C .

2.3 Geometry of two layer deposition for alloy nanoparticles

When depositing with PVD (Physical Vapor Deposition) through a hole mask the hole shrinks due to the material deposited on the edges of the holes. This shrinking results in giving deposited particles the shape of cut of cones instead of cylinders. In general when making alloy nanoparticles by depositing successive layers one wants to achieve a certain ratio in at% between the metals. This taper angle of the particle then needs to be taken into consideration when calculating the height of each layer resulting in certain at% ratio. Previous works, at which detailed calculation is also given [2, 3], have estimated the taper angle to be $\sim 60^\circ$ when using a Lesker PVD 225 Evaporator.

To calculate the height of each layer and achieve certain at% ration between the metals it is easy to calculate the ratio as a function of height and read out the ratio from the resulting graph. The ratio for two layers is given by

$$\frac{n_1}{n_1 + n_2}. \quad (2.6)$$

$n_i = V_i \rho_i$ is the number of particles in each layer i , where V_i is the volume and ρ_i is the density that layer. For cut of cones the volume is given by

$$V_i = \frac{h_i \pi}{3} (r_i^2 + r_i r_{i+1} + r_{i+1}^2). \quad (2.7)$$

Here h_i is the height and r_i and r_{i+1} are the radius of the cones bottom and top respectively. The radii can be calculated from the taper angle α according to

$$r_{i+1} = r_i - \frac{h_i}{\tan(\alpha)}, \quad (2.8)$$

and by knowing the bottom radius from the size of the holes in the hole mask all the radii can be calculated.

Putting these equations together while aiming for a certain total height of the particles we can plot at% of a layer as a function of its height, see figure 2.4. For PdAg

and PdAu disks of size 190 nm x 25 nm the functions are almost identical due to the similarity in volumetric density (I am comparing PdAg and PdAu here since my project started out to analyze both of them but ended up simply analyzing PdAu because of the intriguing results). The functions are also nearly linear since the low particle height gives a fairly low contribution from the taper angle, but just enough to compensate for the difference in volumetric density between Pd and Ag or Au.

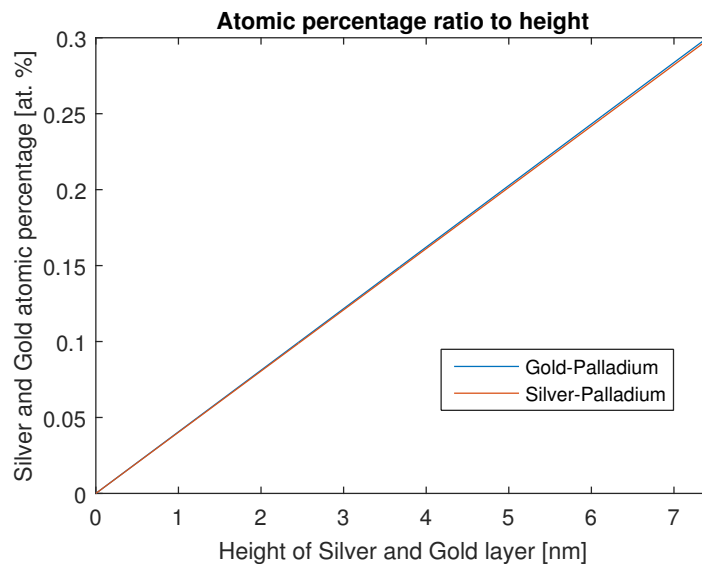


Figure 2.4: The graph shows the calculated atomic percentage of Ag and Au in PdAg and PdAu disks as a function of layer height when first depositing Ag or Au and then Pd. We see that the curves are nearly identical due to Ag and Au having close to the same volumetric density.

3

Experimental methods and HCL fabrication

To measure properties of hydrogen sorption in PdAu nanoparticles I fabricated samples myself using an established method [2,3] adopting the HCL (Holemask Colloidal Lithography) [22] method. The particles were fabricated on both glass and silicon substrates to be able to perform both optical transmission measurements and SEM (Scanning Electron Microscope) characterization. Most measurements were done using a setup measuring optical transmission while varying temperature and hydrogen pressure described in section 3.2. In the following chapter I will go through these methods in detail and explain the process of fabricating and measure hydrogen sorption on PdAu nanoparticle arrays.

3.1 Alloy nanoparticle array fabrication

The fabrication method for creating alloy nanoparticle arrays is illustrated in figure 3.1 and 3.2. The process starts out with preparing substrates of glass or silicon depending on whether optical measurements or SEM will be performed. To remove possible dust or stains the substrates were ultrasonically cleaned together with acetone, isopropanol and water successively. PMMA (Poly(methyl methacrylate)) was then spin-coated onto the substrates for 1 minute with a speed of 2000 rpm resulting in a thickness of ~ 280 nm. Soft baking at 170°C for 10 minutes was then performed to evaporate the solvent and densify the PMMA. To enhance the hydrophilicity of the surface the samples were then exposed to oxygen plasma for 5 seconds.

A layer of positively charged PDDA (poly diallyldimethylammonium) was then drip coated onto the surface which was rinsed of with deionized water and blow dried with nitrogen after 45 seconds of incubation. Negatively charged PS (polystyrene) beads were then attached to the positively charged PDDA surface using the same steps as with the PDDA but with 3 minutes of incubation.

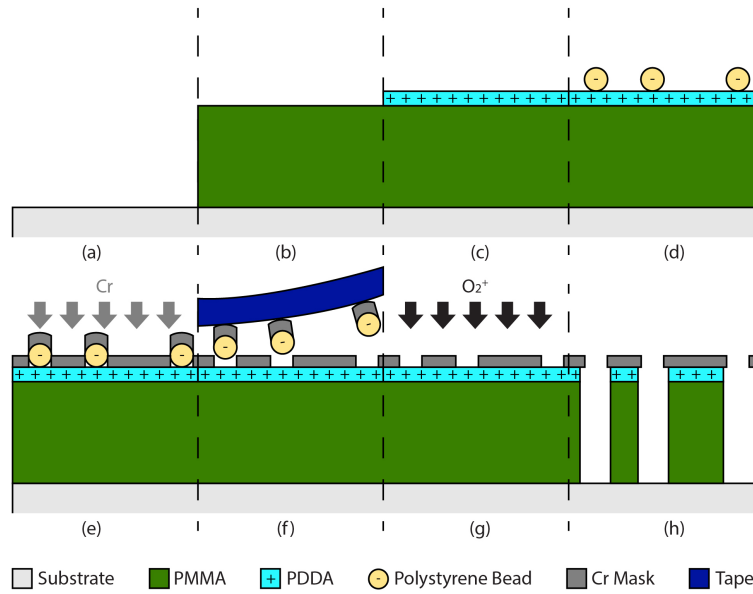


Figure 3.1: (a) Clean substrate. (b) Spin-coated with PMMA. (c) Drip coated with PDDA. (d) Drip coated with PS beads. (e) Evaporation of Cr. (f) Removing PS beads with tape stripping. (g) Oxygen plasma etching. (h) Leaving a holemask ready for deposition of metals to form nanoparticles. The figure is adapted with kind permission from [23].

A Cr film with the thickness of 20 nm was then evaporated onto the sample surface with a Lesker PVD 225 Evaporator at a base pressure of $5 \cdot 10^{-7}$ Torr and an evaporation rate of 1 \AA/s . To remove the PS beads tape stripping was performed, leaving a holemask Cr film on PMMA. Oxygen plasma was then again used, but for 5 minutes, to etch through the PMMA to be able to evaporate metals through the holemask onto the original substrate surface.

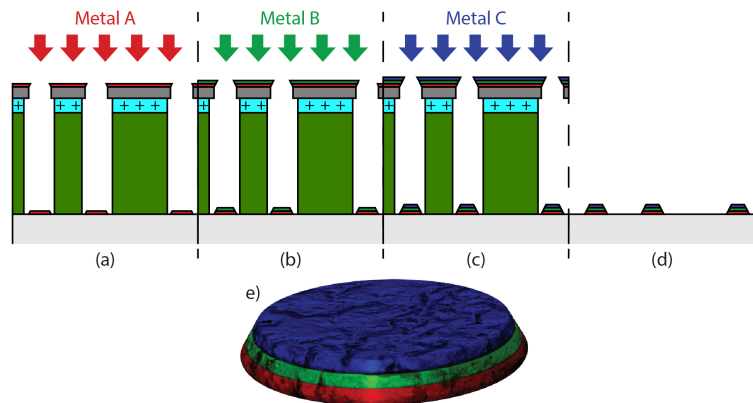


Figure 3.2: (a,b,c) Successive deposition of metals. (d) Lift-off using acetone leaving the substrate with only the metal nanoparticles. (e) An illustration of how a metal layer nanoparticle disk looks after evaporating metals but before annealing it into an alloy. In this thesis, this process was only performed with two layers but the principle is exactly the same. The figure is adapted with kind permission from [23].

With the holmask done, the nanoparticles could be made by successively evaporating desired metals through the hole mask, in my case Pd and Au. The thicknesses of these successive layers were determined by the aimed concentrations of respective metal in the alloy, as well as the taper angle of the disks, see section 2.3 for more details on how to achieve the correct metallic composition. After evaporation, the holmask was removed with lift-off by dissolving the PMMA in acetone. The sample was then annealed in a flow furnace with 4% H_2 in Ar (100 mL min^{-1}) at $500 \text{ }^\circ\text{C}$ for 24 h to form an alloy from the layers of metal.

For more details on materials, substances and equipment used in the fabrication method, see appendix A.1.

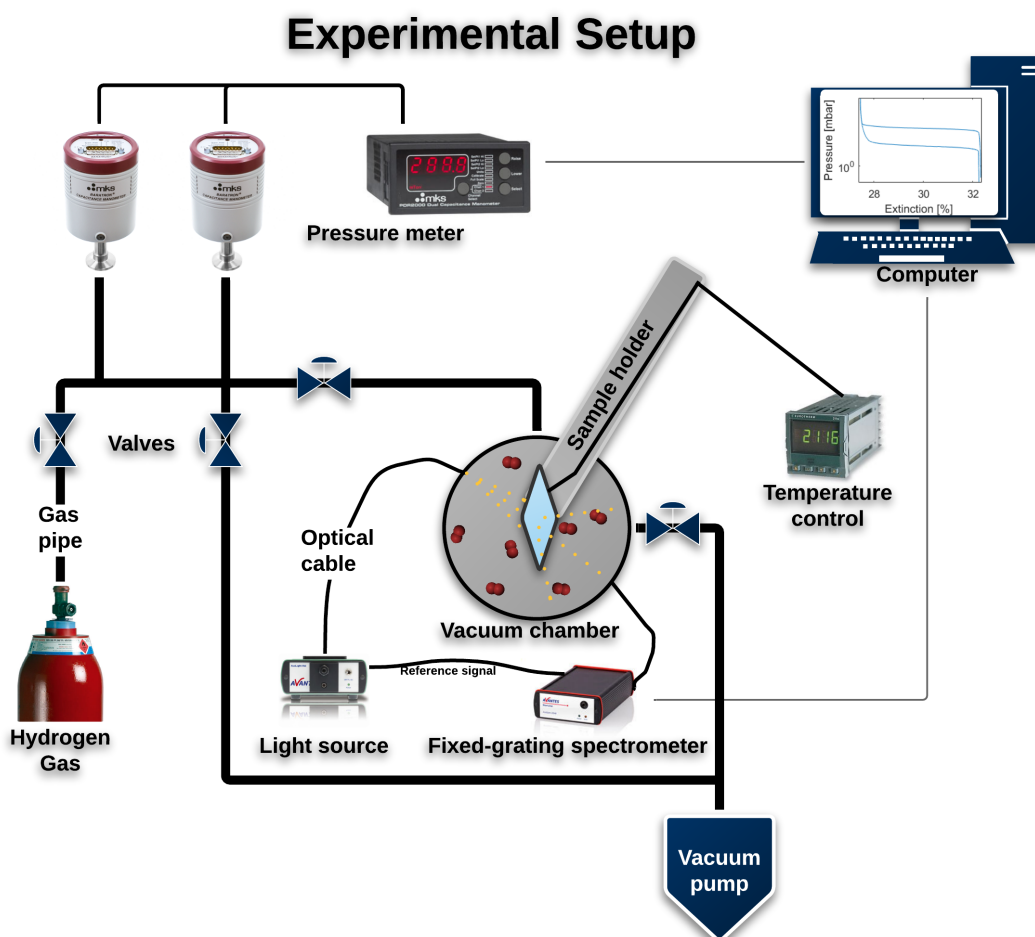


Figure 3.3: The experimental setup for measuring hydrogen sorption is illustrated here. The sample is put into a vacuum chamber where hydrogen gas pressure is controlled and monitored by valves and pressure meters. Light is shone through the sample and compared with a reference signal to get the extinction spectrum and the temperature is kept constant by a thermocouple. The measured values are then transferred to a computer collecting the data.

3.2 Hydrogen sorption measurement setup

To measure energetics and kinetics of hydrogen sorption a homemade vacuum chamber with controlled hydrogen pressure and optical access was used, see figure 3.3. To monitor and control the temperature a thermocouple in direct contact with the sample was used in combination with a temperature controller (Eurotherm 3216N) and a heat coil set up in a feedback loop. In this manner hydrogen measurements at temperatures ranging from 30 to 130 °C were performed. Hydrogen pressure was controlled using a system of valves, and monitored with two capacitive pressure gauges (MKS Baratron Capacitance Manometer). Via an optical access, transmittance through the sample was measured using two UHV(Ultra High Vacuum)-compatible sapphire windows by utilizing a fiber-coupled unpolarized white light source (Avantes AvaLight-Hal) and fixed grating fiber coupled spectrometer (Avantes SensLine AvaSpec-2048XL). The peak wavelength, extinction at the peak and FWHM were then derived by fitting a lorentzian function to the optical spectra during measurement. By plotting these parameters as functions of hydrogen pressure, isotherms were constructed. From these isotherms the energetics of hydrogen sorption could be derived, see subsection 2.2.2. Kinetics was measured in the same way but plotting the position of the LSPR peak versus time instead of pressure.

3.3 Experimental procedure

Several measurement series were performed during this project using similar procedure. First the gold concentrations for the series were chosen and one sample of each concentration was fabricated on glass. One or two concentrations of particular interest were also fabricated on silicon substrates to allow for SEM-characterization. After fabrication the samples were measured one at a time in the hydrogen sorption measurement setup at several temperatures of interest. Two kinds of measurements were done at each temperature. First a slow sweep over hydrogen pressures between 1 μ bar and 1 bar was done to show the hysteresis in hydrogen absorption and desorption. This was done to give data of plateau pressures to calculate energetics and critical temperature. The second kind involved several identical measurements of instantly going from vacuum to 1 bar, waiting until stabilizing and then going instantly back to vacuum. This was done to see how fast the nanoparticles absorb and desorb hydrogen and was also used to evaluate the energy landscape during desorption. If any interesting trend showed from the measured temperatures the same measurements were done at some more temperatures to get higher resolution at the point of interest. The collected data were then analyzed in MATLAB to extract important properties such as energetics, critical temperatures and response times of hydrogen sorption.

Two major measurement series were performed in the way described above. Respective series used PdAu nanoparticles with concentrations of 0, 10, 20 and 30% gold as well as 0, 5, 10, 15, 20, 25 and 30%. I will call these series S1 and S2, respectively, and results from these measurements can be seen in chapter 4.

4

Results and discussion

From the measurement series done in this thesis I have concluded that the critical temperature decreases gradually from $\sim 250^\circ\text{C}$ to somewhere close to room temperature when increasing gold concentration from 0 to 30% in PdAu alloy nanodisks of the size 190 nm x 25 nm annealed in a flow of 100ml/min of 4% H₂ in Ar at 500°C for 24 h. The response time t_{90} when going from 1 bar to vacuum decreases from 62 s to ~ 10 s for the same increase in gold concentration, while the response time for absorption decreases from 1.5 s to ~ 0.5 s. I have also shown that the energy landscape of absorption and desorption can be extracted from kinetic measurements. I will now present these results and discuss how they can be interpreted.

4.1 Energetics

By plotting the extinction spectra of PdAu nanoparticles while absorbing and desorbing hydrogen I could obtain the isotherm measurement series shown in figure 4.1 and 4.2. For convenience I will call these series S1 and S2, respectively. S1 is a series of samples with gold compositions of 0, 10, 20 and 30 at%, while S2 has the compositions 0, 5, 10, 15, 20, 25 and 30 at%. Both series were measured on samples fabricated in the same way according to the fabrication method described in section 3.1. In both measurement series a pronounced transition region between α and β -phase is seen for compositions with low amount of gold. This transition region diminishes with the increase of gold while α and β -phase regions broaden. At the same time the absolute signal shift decreases, which is the main drawback with increasing the gold concentration since it decreases the signal to noise ratio. At compositions with 20% gold the phase transition region is already gone at room temperature and increasing the amount of gold to 30% further linearize the response which is preferable for sensing applications.

A slight deviation in the trend of diminishing phase transition regions is seen for 25% gold in measurement series S2, shown in figure 4.2. It shows a more prominent hysteresis at phase transition which is not expected for this alloy composition annealed for 24 hours. Instead it follows closely to earlier measurements for samples annealed for 6 hours. Speculatively, it may be that particles with 25% gold have reached a preferred crystal structure already after 6 hours of annealing and do not change further with more annealing time. However, additional samples should be made to verify that this is a reproducible result and not simply an artifact.

Other than the expected hysteresis at the transition between α and β phase, a hysteresis beyond the phase transition region is seen, spanning nearly throughout

all pressures. This overall hysteresis is not seen for the same kind of nanoparticles annealed for 6 hours [2] and is more prominent for S2, see figure 4.2. The cause of this hysteresis is not totally clear and could have many explanations. Among the possible explanations substrate-particle strain is probably the most likely. Prior research [16] has shown that the plateau pressure of hydrogen absorption slopes due to different strain in different parts of the sample. Because of the variation in strain there would be a variation in plateau pressure resulting in a sloping plateau. In our case, this may be caused by a difference between nanoparticles or within individual nanoparticles (different hydrogen absorption sites such as surface or bulk). This phenomenon is however, as said before, not seen for the same particles annealed for 6 hours. Therefore a difference between particles is probably not the case, since additional annealing time should make the particles more alike. The additional annealing time may instead increase the difference in strain even further between surface and bulk sites within individual particles as well as increasing the strain on the substrate-particle interface. This variation in strain may then extend the hysteresis to even higher and lower pressures.

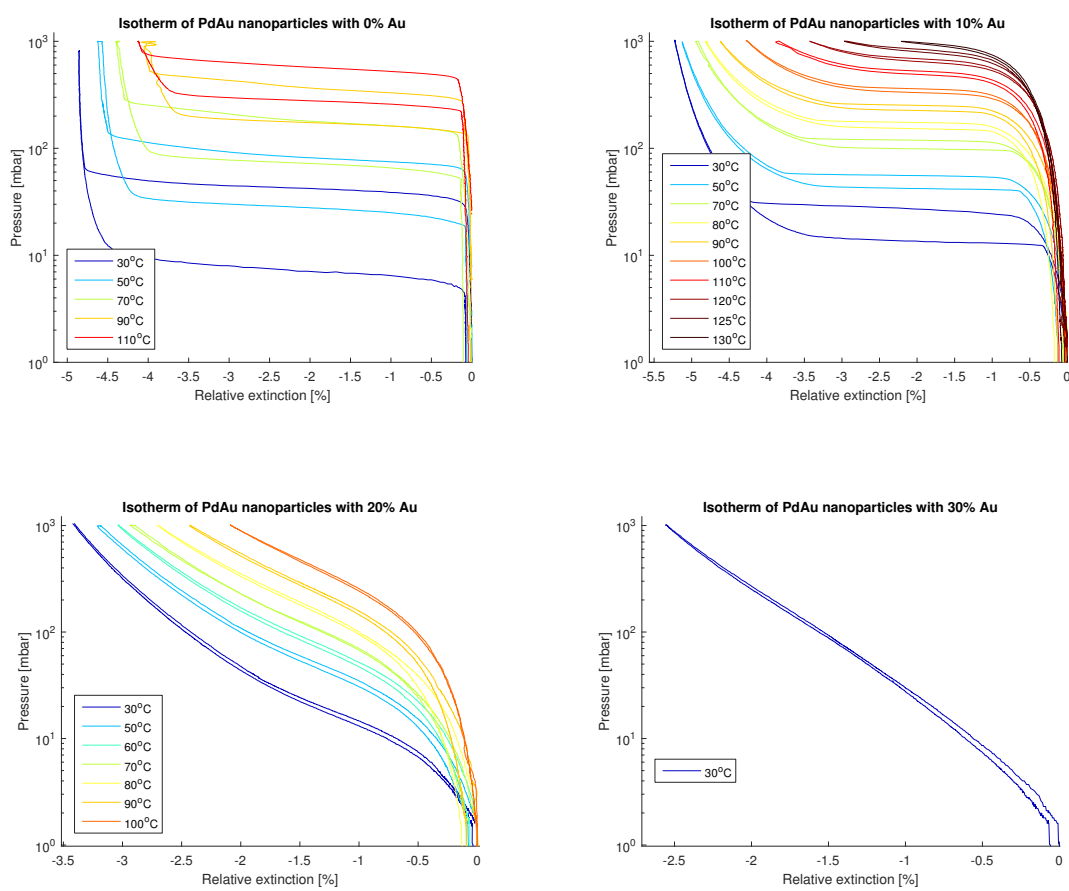


Figure 4.1: The figure shows the first measurement series (S1) of isotherms for PdAu nanoparticles with varying amount of gold, 0, 10, 20 and 30%, and at different temperatures. As the temperature rises the hysteresis decreases and for higher concentrations of gold there is nearly no hysteresis already at room temperature. Here the extinction at peak position is showing how much hydrogen is absorbed. For the same series but with relative peak position, see appendix A.2.

4. Results and discussion

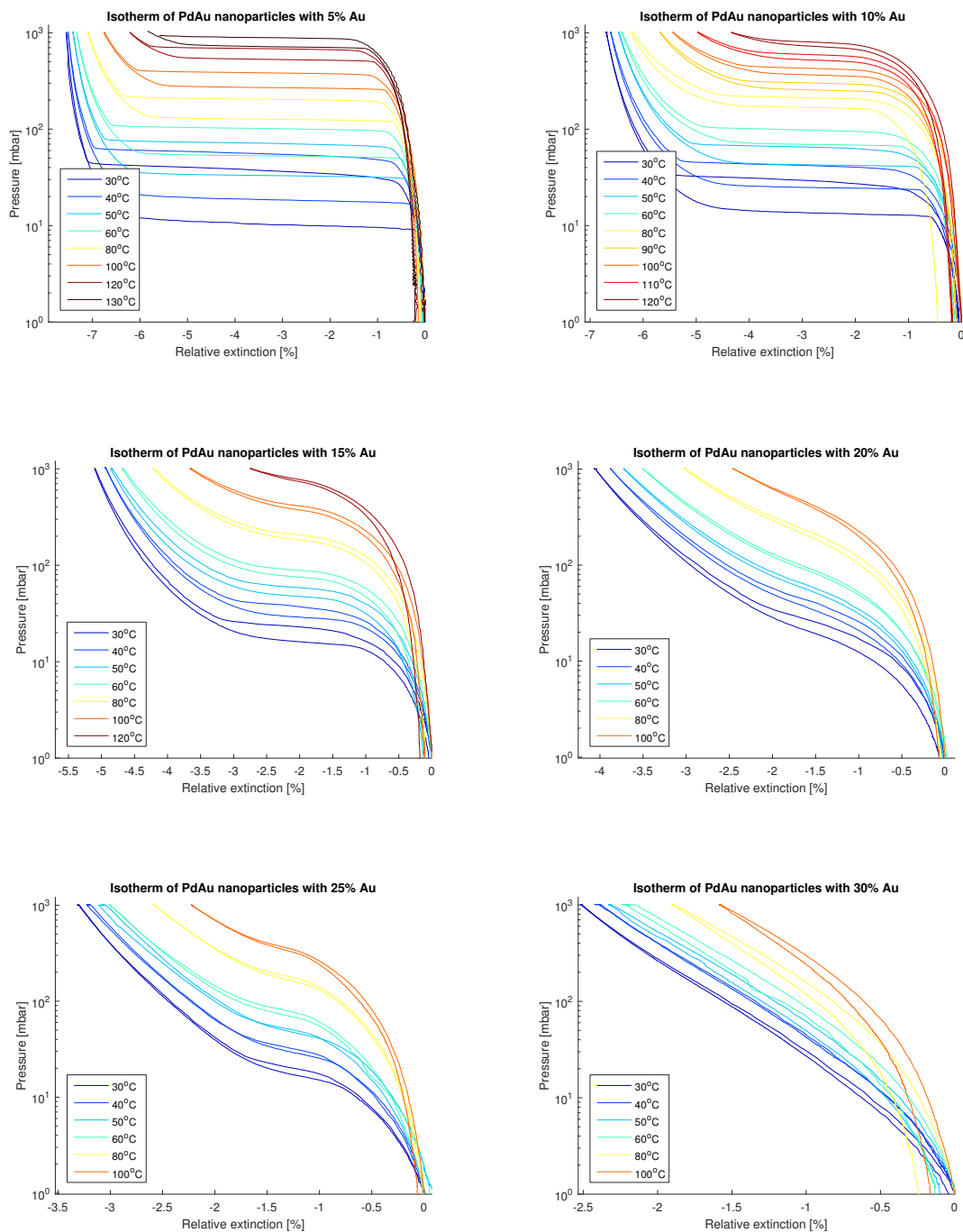


Figure 4.2: The figure shows the second measurement series (S2) of isotherms for PdAu nanoparticles with varying amount of gold, 5, 10, 15, 20, 25 and 30%, and at different temperatures. The general shapes of the isotherms are very similar to S1 indicating reproducibility. The measurements at 25% gold are a bit out of the trend and show a more prominent hysteresis at phase transition. Further research should look into if this is simply happenstance or if this may be some phenomenon related to crystal structure. Also here the extinction at peak position is showing how much hydrogen is absorbed. For the same series but with relative peak position, see appendix A.2. For the measurement of 0% gold in this series see figure A.3

Other speculative explanations for the overall hysteresis may be particle aggregation, variation in crystal structure between particles or rearrangement of crystal structure during absorption and desorption. Measurements on single nanoparticles would here be very useful to determine whether the same kind of hysteresis is seen for single particles and narrow down the possible reasons for the phenomenon. Furthermore cycling between measuring and annealing for longer times or at higher temperatures would be a good way of analyzing how and when this kind of hysteresis occurs.

4.1.1 Critical temperature

The critical temperature was determined in two ways. First using the Van't Hoff model [20] and then by fitting the hysteresis width with data collapse [21]. Calculated values for the critical temperature are displayed in figure 4.6 and table 4.1.

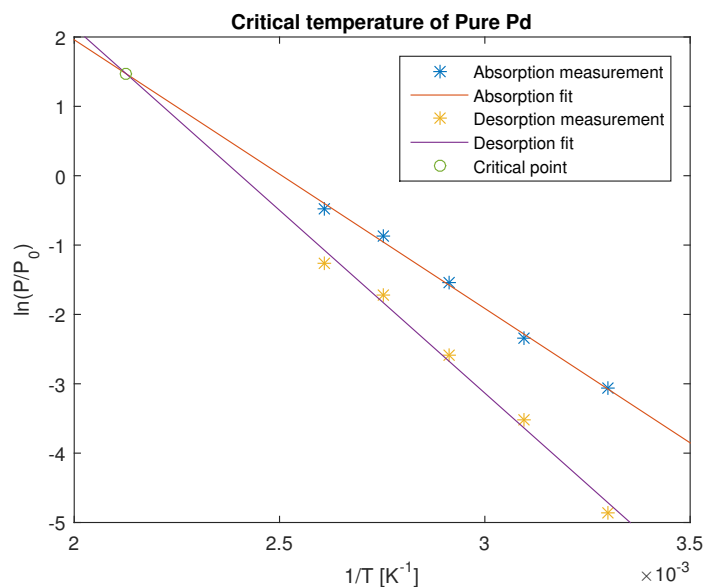


Figure 4.3: A typical Van't Hoff plot showing how the gap between enthalpy of absorption and desorption decreases until the critical temperature is reached. In this particular example it is used to calculate the critical temperature of pure Pd nanoparticles, giving a value of 197.4°C. Additional Van't Hoff plots used in this thesis are found in appendix A.4.

By fitting the logarithm of plateau pressures from the isotherms in figure 4.1 and 4.2 to Van't Hoff's equation, graphs such as the ones shown in figure 4.3 were created. Here linear curves are fitted to the constants $\ln(K_{eq})$ of absorption and desorption (i.e. plateau pressures) at different temperatures. By finding the intersection between these curves the critical temperature is determined. This method gives a good approximation of T_C , which can be seen when the value for T_C reaches temperatures and pressures within measurable range of our setup. Comparing the graph for 10% gold in figure 4.1 the slope of the phase transition plateaus becomes more and more pronounced after $\sim 100^\circ\text{C}$ typical for passing the critical temperature. At the same time the T_C value calculated is 101.6°C which is very reasonable.

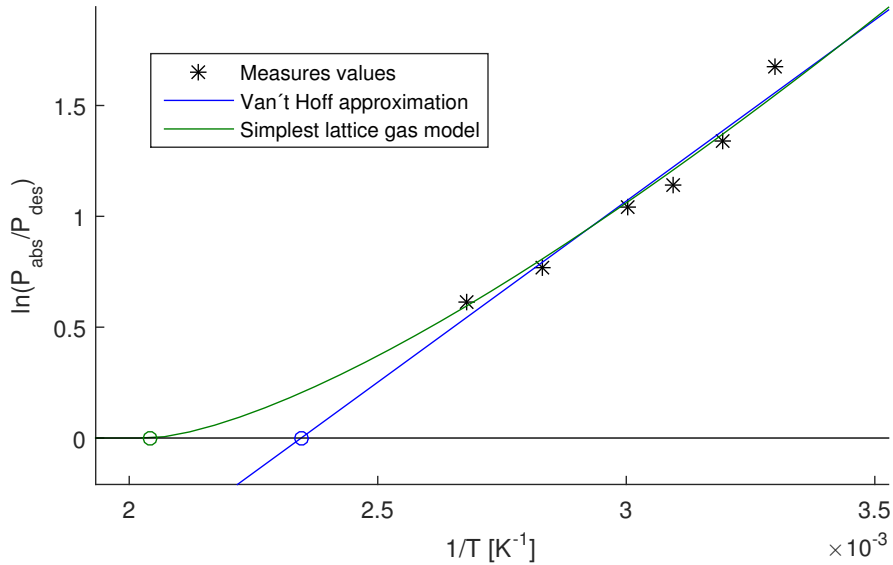


Figure 4.4: Two different ways to determine the critical temperature with either Van't Hoff analysis or the simplest lattice gas model with linear H-H interactions is shown above. The comparison demonstrates how the linear approximation of the Van't Hoff equation underestimates the critical temperature for measurements far away from T_C . The figure is adapted from reference [21].

However, the linear approximation in Van't Hoff's equation is not totally accurate far away from T_C as is illustrated in figure 4.4. When comparing to the simplest lattice gas model where linear H-H interactions are taken into account, we see that T_C from the Van't Hoff equation is significantly underestimated when approximated with values far away from T_C . This is caused by neglecting the influence of H-H interactions. Because of this underestimation, together with the overall hysteresis seen in my measurement, the reliability of the Van't Hoff method is unclear. Since the overall hysteresis does not diminish to the same extent when the temperature is increased the outcome with Van't Hoff analysis becomes very uncertain and does not give a reliable result for higher concentrations of gold. Such an example is seen for 15% gold of the measurement series S2, see table 4.1. At higher concentrations the overall hysteresis is even more prominent than the hysteresis at phase transition, possibly due to that we are already above T_C . This makes it impossible to determine T_C from Van't Hoff analysis and therefore another way of evaluating T_C was performed. This was done both to be able to compare differences and discuss how to evaluate T_C for alloy nanoparticles as well as to try and determine T_C for higher concentrations of gold.

Table 4.1: The table shows critical temperature values from the two different methods of calculating T_C . The value calculated with Van't Hoff analysis for 15% gold diverges from the trend, probably due to the large overall hysteresis in comparison with the normal hysteresis. The squares without values are not possible to calculate with Van't Hoff's equation due to the overall hysteresis.

Measurement series	S1			S2						
Gold concentration [%]	0%	10%	20%	0%	5%	10%	15%	20%	25%	30%
T_C from Van't Hoff [°C]	197.4	101.6	-	153.1	147.3	127.1	146.3	-	-	-
T_C from spinodal fit [°C]	271	141	97.6	225.9	189.8	140.7	103.7	103.9	88.2	103.1

The second method of finding the critical temperature was to fit the hysteresis height of the measured isotherms to equation (2.2.3), see subsection 2.2.3 for more details. The scaling factor of this equation is different for different materials but is assumed to be the same for my series of nanoparticles. With this assumption the hysteresis width from nanoparticles of different concentrations scale in the same way with respect to the temperature relative to T_C . Since the the hydrogenation of the nanoparticles is still driven by Pd and there is no difference in size or shape between the different concentrations it is probably a sound assumption.

Since the equation scales with T_C/T , where T is the measurement temperature, the data for all concentrations may be collapsed unto the same curve to find the best collective fit. Such an evaluation with data collapse is displayed in figure 4.5.

This technique also have troubles with the overall hysteresis giving slightly higher values of T_C since this hysteresis is added to the distance between absorption and desorption plateaus. Because of this, the method is unable to resolve the critical temperature below $\sim 100^\circ\text{C}$. However, it might instead be seen as an upper limit for T_C at high concentrations of gold.

Looking only at the lower gold concentrations, 15% and below, the data collapse method gives a very reasonable result. Comparing the calculated T_C s from table 4.1 with the graphs in figure 4.2 the calculated values are certainly in the region we expect them to be just from looking at how the hysteresis decreases and the plateau slope changes. Especially the values of both $T_C = 140.7^\circ\text{C}$ for 10% gold and $T_C = 103.7^\circ\text{C}$ for 15% gold are in good agreement with the shape of the isotherms. This indicates that the method is accurate, at least for lower gold concentrations.

A summary of calculated critical temperatures is seen in figure 4.6. The trend of decreasing critical temperature with increasing gold concentration is very clear. However, none of the methods are able to give a good approximation for higher gold concentrations due to the overall hysteresis. The spinodal fit works best in this regard giving at least an upper limit instead of not being able to give a value at all.

Knowing that the shape of the non-linearity in Van't Hoff's equation gives a slightly lower value of T_C , while at the same time noticing the overall hysteresis gives a higher value for T_C is of interest when comparing the two different techniques. Because of this, they may together be used to give a lower and an upper limit for the critical temperature.

4. Results and discussion

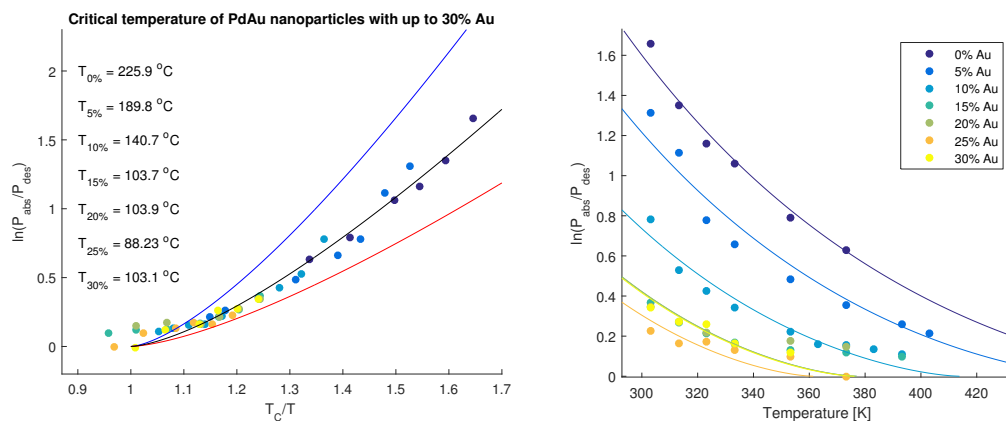


Figure 4.5: To the left we see the critical temperatures of a series of PdAu nanoparticles calculated with data collapse, assuming the spinodal fits will scale with the same k-factor. To the right the same values are shown but to the scale of the absolute temperature instead of the temperature relative to individual T_C . These graphs display the analysis for S2. However, data collapse was also done on S1, shown in appendix A.5.

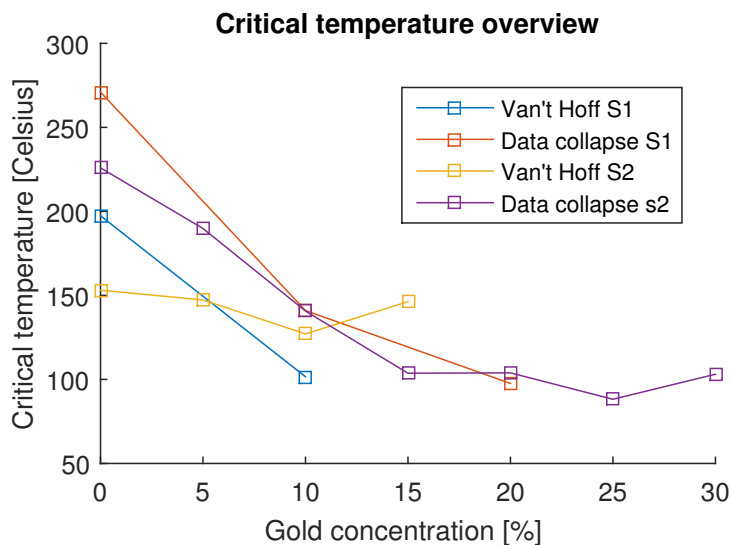


Figure 4.6: The graph shows a summary of calculated critical temperatures with the values seen in Table 4.1. A general trend is seen with T_C decreasing from slightly above 200°C down to around 100°C . The Van't Hoff method on S2 shows a low value for 0% gold, probably due to only using temperatures up to 100°C resulting in an underestimation from the linear approximation of the method far from T_C .

Enthalpy and entropy of absorption and desorption were also calculated from the Van't Hoff analysis. These results are displayed in table 4.2. However, only for concentrations of gold up to 15% since Van't Hoff analysis did not work for higher concentrations. This is due to the overall hysteresis becoming more prominent than the phase transition hysteresis at higher concentrations. The general trend for these results is that the change in enthalpy and entropy increases for absorption but de-

creases for desorption as the gold concentration increases. This is probably because absorption and desorption becomes more alike for increased gold concentration as the hysteresis diminishes.

Table 4.2: Energetics for PdAu of different alloy concentrations calculated with Van't Hoff analysis. Values for higher gold concentrations were not possible to calculate due to the increasing overall hysteresis.

Measurement series	S1		S2			
	0%	10%	0%	5%	10%	15%
Gold concentration [%]	0%	10%	0%	5%	10%	15%
dS Abs. [$\frac{J}{K \cdot mol}$]	80.8	83.0	78.4	79.0	91.1	95.7
dH Abs. [$\frac{kJ}{mol}$]	-32.2	-34.4	-31.0	-32.4	-36.7	-38.5
dS Des. [$\frac{J}{K \cdot mol}$]	105.4	104.4	110.3	103.8	107.9	100.9
dH Des. [$\frac{kJ}{mol}$]	-43.8	-42.4	-44.6	-42.8	-43.4	-40.7

4.2 Kinetics

By reading the change in extinction when suddenly changing the pressure either from vacuum (a few μbar) to 1 bar or back from 1 bar to vacuum, the kinetic properties of the PdAu nanoparticles were measured. From these measurements the response time in which the system catches up to its surroundings can be determined, as well as the energy landscape for the rate-limiting step (associative H_2 desorption from the surface) along the reaction coordinate. Such a measurement can be seen in figure 4.7, where the rate of absorption and desorption are compared alongside each other.

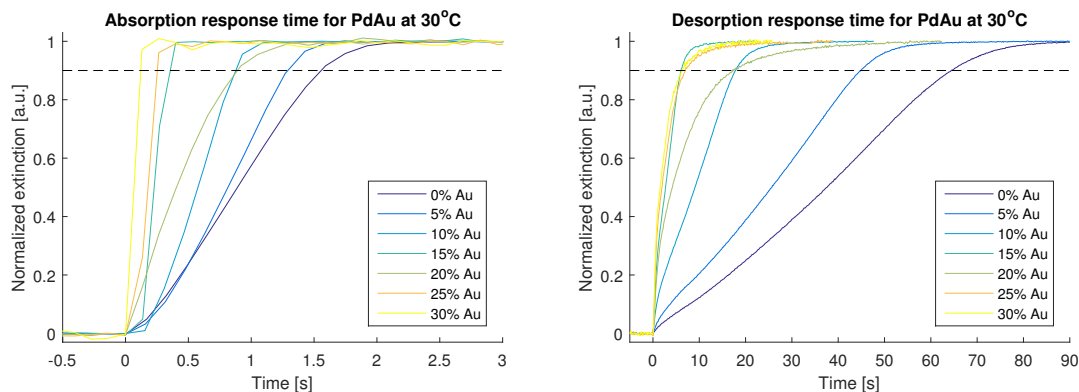


Figure 4.7: Both graphs show the normalized extinction when absorbing (to the left) or desorbing (to the right) hydrogen, going from vacuum to 1 bar or from 1 bar to vacuum. The increase in speed with increased gold concentration is very clear as well as the fact that the desorption process is slower than the absorption process.

From the extinction curves in figure 4.7 the response time t_{90} in which the system has reached 90% saturation can be evaluated. A summary of the response time for both absorption and desorption is seen in figure 4.8. The response time is decreasing

with increasing gold concentration except for an unexpected peak at 20% gold. This peak is probably a deviation in this particular sample but measurements on another sample of 20% gold would be good to establish this. The overall trend of decreasing response time is however very clear.

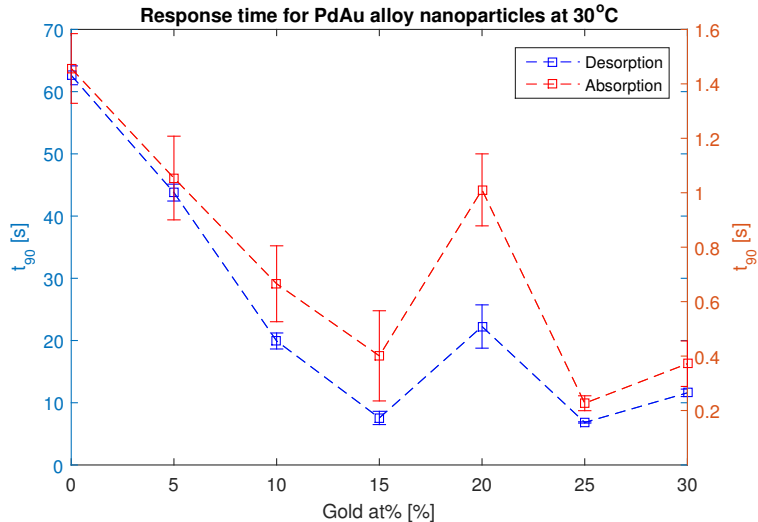


Figure 4.8: A summary of the response time for PdAu nanoparticles of varying gold concentration is seen in the graph above. The trend of increasingly faster kinetics with higher gold concentration is clear. However, the value at 20% gold is deviating from the trend.

4.2.1 Energy landscape

From the kinetic data, the activation energy evolution while decreasing the amount of hydrogen can be evaluated. This was obtained by applying Arrhenius analysis [24] for each time step decreasing the amount of hydrogen concentration by 1 %. From these activation energies a quantitative description of the energy landscape of the evolution of the activation barrier for associative H_2 desorption from the surface was extracted. The reason to use desorption is that it is slower than absorption which gives higher resolution, while the absorption speed is too fast for us to resolve any proper result with our setup. The result from such analysis is visualized in figure 4.9.

From the shape of the energy landscapes one can distinguish the different phases with a phase transition region in between. As the gold concentration increases α and β phases become more and more prominent on either side, diminishing the phase transition region.

Another interesting trend from the calculated energies is the decrease in energy barrier with increased gold concentration. At lower gold concentrations slight increase is seen but for higher concentrations the energy decreases steadily. These results go well together with the decreasing response time.

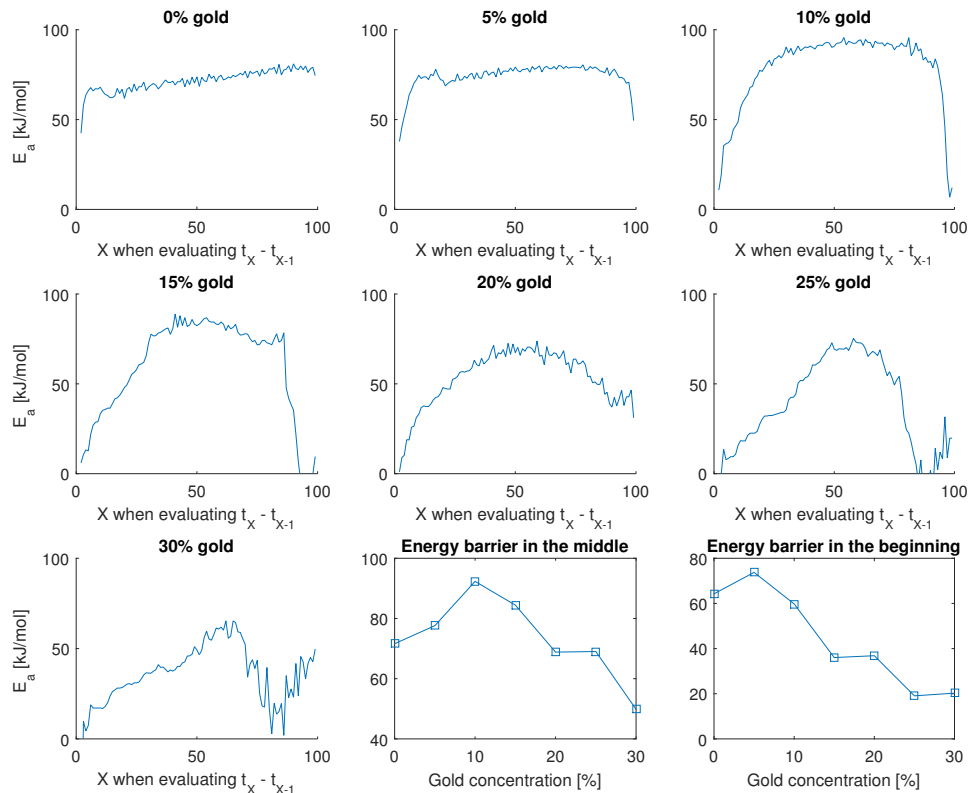


Figure 4.9: A series of graphs displaying the energy landscape of the evolution of the activation barrier for associative H_2 desorption from the surface for samples with increasing the gold concentration. The energy increases for the first few steps of increase in gold concentration, but then decreases steadily.

4.3 Relation between extinction spectrum descriptors

As a final result I would like to highlight the amount of information that is stored in measurements of the extinction spectrum. Since the whole extinction spectrum is measured for every single data point on the curve going from a few μbar to 1 bar and vice versa, a lot more information than just the peak position or extinction at the peak can be extracted. This could be utilized to see how well different ways of modelling nanoparticles describe the extinction spectrum as has been done by Poyli et al. [25]. Poyli et al. derived the dielectric function for Pd nanodisks with different approximations and observed the behavior of the resulting extinction spectrum. From this they could conclude that the hydrogen saturation of the disks took place at ~ 0.667 H/Pd in β phase, as well as demonstrating that the sensitivity of plasmonic sensing techniques is enough to study dynamics of structural changes in metal hydride nanosystems.

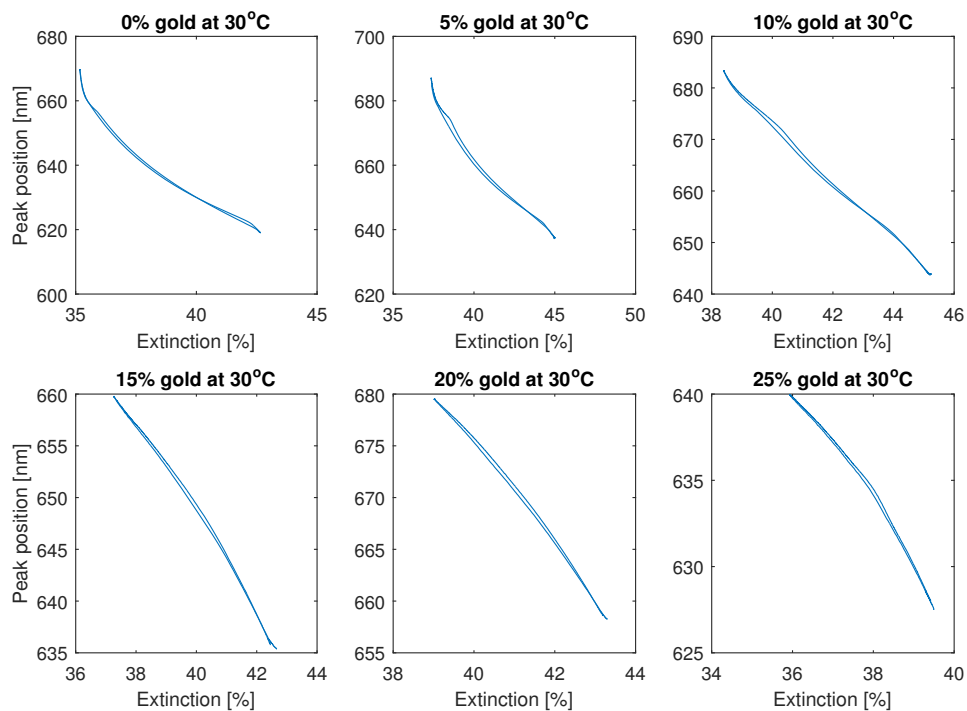


Figure 4.10: The graphs compare the two descriptors, peak position and extinction at peak position for the measurements at 30°C presented in figure 4.2. This kind of comparisons can be done with FWHM as well and may also be done at all temperatures, see appendix A.3. The information stored in this data may very well provide for better understanding of the plasmonics of metal hydride alloy nanoparticles.

To show how similar approaches could be done with my measurements I display peak positions plotted as function of extinction at peak position in figure 4.10. We here see a gradual change in the relation between these quantities as the gold concentration of the nanoparticles increases. Seeing how the graphs are significantly different in shape depending on gold composition suggests a difference in how the descriptors relate to the hydrogen concentration. These exact trends have been observed before, see figure A.15 in appendix A.3, indicating a real effect. Most likely the different descriptors read out different responses for various absorption sites. Therefore, this can be used to get information about how the sorption hydrogen occurs in the particles combined with preferences for different sites in the nanoparticles such as surface, bulk or various defects. This kind of data is available for a variety of temperatures and the relations to FWHM may also be used in the same way to create three times the amount of data by relating it to both peak position and extinction. All these relations together very well describe the shape of the total extinction spectrum and can be put in use to establish models describing the hydrogen absorption and diffusion in metal hydride alloys and their plasmonic behavior.

5

Conclusions

In this thesis I have shown how PdAu alloy nanoparticles can be used for hydrogen sensing and how various properties of hydrogen sorption in these particles can be characterized. I have discussed two different methods of determining critical temperature, analyzed the response times and given a quantitative description of the energy landscape for alloy concentrations with up to 30% gold. I have also pointed out that large amount additional information about plasmonic properties may be stored in the measurement data since the whole extinction spectrum is measured. The amount of data as well as the quality of the data goes to show how powerful of a technique plasmonic sensing is. And even though there are a lot of unanswered questions generated by the results we see, we have a great tool to provide the answers.

The main question mark is probably: What causes the overall hysteresis? This is a question that will not be answered in this thesis since more research is needed to narrow down possible explanations in order to establish a proper theory. However, measurements on single particles as well as mapping the influence of annealing time and temperature are already on the way and may hopefully give us an answer in the near future.

From my results it is not obvious if I have found a suitable method to determine the critical temperature of alloy nanoparticles. However, using several methods seems to be a good way to validate the results to some extent, while providing input for discussion on why some methods may deviate from the correct result. To some extent the Van't Hoff method and the data collapse method may very well work together to form a lower and an upper limit for the critical temperature. Though, this is mainly in the case of overall hysteresis causing the data collapse to slightly overestimate the critical temperature.

A common trend for all measurements is better properties for sensing with increased gold concentration, except for the one drawback with decrease in signal strength. Even so, higher concentrations will most likely not give better results for sensing applications, since the hysteresis is principally gone at 30% gold and other improvements such as response time and activation energy do not improve as much for higher concentrations as they do at low concentration. Hence, higher concentrations are probably not very likely to give interesting results.

5.1 Outlook

The outcome of this thesis shows that we still have a lot to learn about PdAu nanoparticles, perhaps leaving us with more questions than we had before. But this is just the more reason to continue researching the field since it is the things we do not know that are possible to discover.

From my point of view the way to proceed, as I have mentioned before, is to study single nanoparticles as well as varying annealing time and temperature in order to figure out the cause of the overall hysteresis. Especially I think the methodology of measuring samples annealed for a short time and then anneal them again for a longer time would be a great way to investigate whether the overall hysteresis is only due to the annealing time.

Another interesting prospect is to measure samples of 20% gold concentration and above, below room temperature to find the temperature where the phase transition hysteresis becomes prominent. This would establish that we are indeed below the critical temperature at room temperature and that the small hysteresis seen is due to some other effect. It would also be useful in order to see more clearly how the critical temperature depends on gold concentration.

Furthermore the energy landscape results as well as the information contained in the extinction spectrum can be combined with simulations and theoretical models to establish detailed understanding of these systems also on a theoretical level.

We may not know if all of these ideas will be attempted or what result they may bring, but one thing is certain. There are many ways to continue researching this area and it will be very interesting to see what the future brings.

Bibliography

- [1] Crabtree1, G. W., Dresselhaus, M. S. and Buchanan M. V. (2004) The hydrogen economy. *Physics Today*, vol 57, issue 12, pp 39-44. DOI: <http://dx.doi.org/10.1063/1.1878333>
- [2] Wadell, C., Nugroho, F. A. A., Lidström, E., Iandolo, B., Wagner, J. B. and Langhammer, C. (2015) Hysteresis-Free Nanoplasmonic Pd–Au Alloy Hydrogen Sensors. *Nano letters*, vol. 15, issue 5, pp 3563–3570.
- [3] Nugroho, F. A. A., Iandolo, B., Wagner, J. B. and Langhammer, C. (2016) Bottom-Up Nanofabrication of Supported Noble Metal Alloy Nanoparticle Arrays for Plasmonics. *ACS Nano*, vol. 10, issue 2, pp 2871–2879 DOI: 10.1021/acsnano.5b08057
- [4] Lewis, F. A. (1960) The Hydrides of Palladium and Palladium Alloys. *Platinum Metals Rev.*, vol 4, issue 4, pp 132.
- [5] Lewis, F. A. (1994) The palladium-hydrogen system: structures near phase transition and critical points. *International Journal of Hydrogen Energy*, vol 20, issue 7, pp 587–592. doi:10.1016/0360-3199(94)00113-E
- [6] Brongersma, M. L. (2015) Introductory lecture: nanoplasmonics. *Faraday Discuss*, vol 178, pp 9-36. DOI: 10.1039/C5FD90020D
- [7] Nakayama, K., Tanabe, K. and Atwater, H. A. (2008) Plasmonic nanoparticle enhanced light absorption in GaAs solar cells. *Appl. Phys. Lett.*, vol 93, issue 12, pp 1904. <http://dx.doi.org.proxy.lib.chalmers.se/10.1063/1.2988288>
- [8] Sotiriou, G. A., Starsich, F., Dasargyri, A., Wurnig, M. C., Krumeich, F., Boss, A., Leroux, J. and Pratsinis, S. E. (2014) Cancer Treatment: Photothermal Killing of Cancer Cells by the Controlled Plasmonic Coupling of Silica-Coated Au/Fe₂O₃ Nanoaggregates. *Advanced Functional Materials*, vol 24, issue 19, pp 2818-2827. DOI: 10.1002/adfm.201470124
- [9] Das, S. and Turunen, J. (2012) Plasmonic nanosensors in the treatment of cancer: an attempt to conquer the immortal illness. *SPIE Proceedings*, vol 8424. doi:10.1117/12.916701
- [10] Kreibig, U., Vollmer, M. (1995) *Optical Properties of Metal Clusters*. Berlin: Springer-Verlag.
- [11] Mie, G. (1908) Beiträge zur Optik trüber Medien, speziell kolloidaler Metallösungen, *Ann. Phys.*, vol 25, pp 377-445 .
- [12] Ashcroft, N., Mermin, N. D. (1976) *Solid State Physics*. Saunders College. pp 2–6.
- [13] Zoric, I., Larsson, E. M., Kasemo, B. and Langhammer, C. (2010) Localized Surface Plasmons Shed Light on Nanoscale Metal Hydrides. *Adv. Mater.*, vol 22, issue 41, pp 4628–4633. doi:10.1002/adma.201000973

- [14] Graham, T. (1869) On the Relation of Hydrogen to Palladium. *Proc. Roy. Soc.*, vol 17 , pp 212–220.
- [15] Lide, D. R. and Frederikse, H. P. R. (1993-94) *CRC Handbook of Chemistry and Physics*. 74th edn. Boca Raton, FL: CRC Press
- [16] Wagner, S. and Pundt, A. (2015) Quasi-thermodynamic model on hydride formation in palladium-hydrogen thin films: Impact of elastic and microstructural constraints. *International Journal of Hydrogen Energy*, vol 41, issue 4, pp 2727–2738. doi:10.1016/j.ijhydene.2015.11.063
- [17] Syrenova, S. et al. (2015) Hydride formation thermodynamics and hysteresis in individual Pd nanocrystals with different size and shape. *Nature Mater.* Issue 14, pp 1236–1244. <http://dx.doi.org/10.1038/nmat4409>
- [18] Schwarz, R. B. and Khachatryan, A. G. (1994) Thermodynamics of Open Two-Phase Systems with Coherent Interfaces. *Phys. Rev. Lett.*, vol 74, issue 13, pp 2523-2526. DOI:<http://dx.doi.org/10.1103/PhysRevLett.74.2523>
- [19] Bérubé, V., Radtke, G., Dresselhaus, M. and Chen, G. (2007) Size effects on the hydrogen storage properties of nanostructured metal hydrides: A review. *International Journal of Energy Research*, vol 31, issue 6-7, pp 637–663. DOI: 10.1002/er.1284
- [20] Van't Hoff, M. J. H. (1884) Etudes de dynamique chimique. *Recueil des Travaux Chimiques des Pays-Bas*, vol 3, issue 10, pp 333–336.
- [21] Griessen, R., Strohfeldt, N. and Griessen, H. (2015) Thermodynamics of the hybrid interaction of hydrogen with palladium nanoparticles. *Nature Materials*, vol 15, issue 3, pp 311-317 DOI: 10.1038/NMAT4480
- [22] Fredriksson, H., Alaverdyan, Y., Dmitriev, A., Langhammer, C., Sutherland, D. S., Zäch, M. and Kasemo, B. (2007) Hole–Mask Colloidal Lithography. *Advanced Materials*, vol 19, pp 4297–4302. doi:10.1002/adma.200700680
- [23] Ferry, N.(2016) Nanoplasmonic Sensing of Materials for Energy Applications. Thesis for the degree of licenciate of engineering.
- [24] Laidler, K. J. (1987) *Chemical Kinetics*, Third Edition, New york: Harper & Row, pp 42.
- [25] Poyli, M. A., Silkin, V. M., Chernov, I. P., Echenique, P. M., Muiño R. D. and Aizpurua, J. (2012) Multiscale Theoretical Modeling of Plasmonic Sensing of Hydrogen Uptake in Palladium Nanodisks. *J. Phys. Chem. Lett.*, vol 3, issue 18, pp 2556–2561. DOI: 10.1021/jz3007723

A

Appendix 1

A.1 HCL alloy fabrication details

Here additional details about materials, substances and equipment used in the HCL alloy fabrication method is presented:

Glass: Borofloat, Schott Scandinavia AB

PMMA: from MicroChem Corporation, 4 wt % diluted in anisole, MW = 950 000

PDDA: MW = 200 000-350 000, Sigma-Aldrich, 0.2 wt % in Milli-Q water, Millipore

PS beads: 190 ± 6 nm, sulfate latex, Interfacial Dynamics Corporation, 0.2 wt, % in Milli-Q water, Millipore

Oxygen plasma: 50 W, 250 mTorr, Plasma Therm Batchtop RIE 95m

Tape stripping: with tape SWT-10, Nitto Scandinavia AB

A.2 Additional isotherms

Since both peak position and extinction at peak position were analyzed in the thesis the isotherms of measurement series S1 and S2 are shown for peak position in figure A.2 and A.1. Also the isotherms from S2 with 0% gold can be seen in figure A.3 for both extinction and peak position.

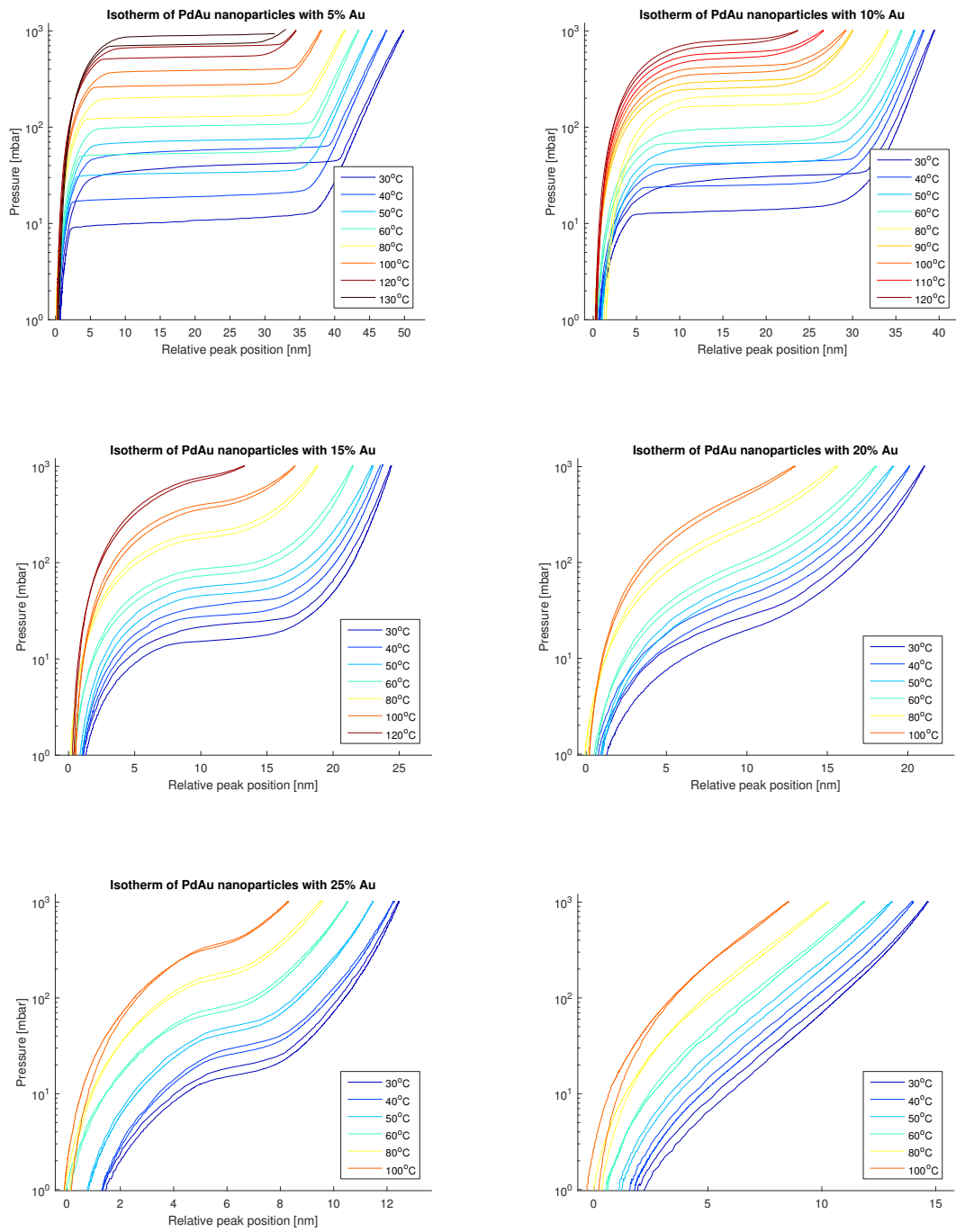


Figure A.1: The figure shows the second measurement series (S2) of isotherms for PdAu nanoparticles with varying amount of gold, 5, 10, 15, 20, 25 and 30%, and at different temperatures, but extracted from peak position instead of extinction. Also here, both ways of interpreting the data show the same trends but with slight variation in shape. For 0% gold see figure A.3

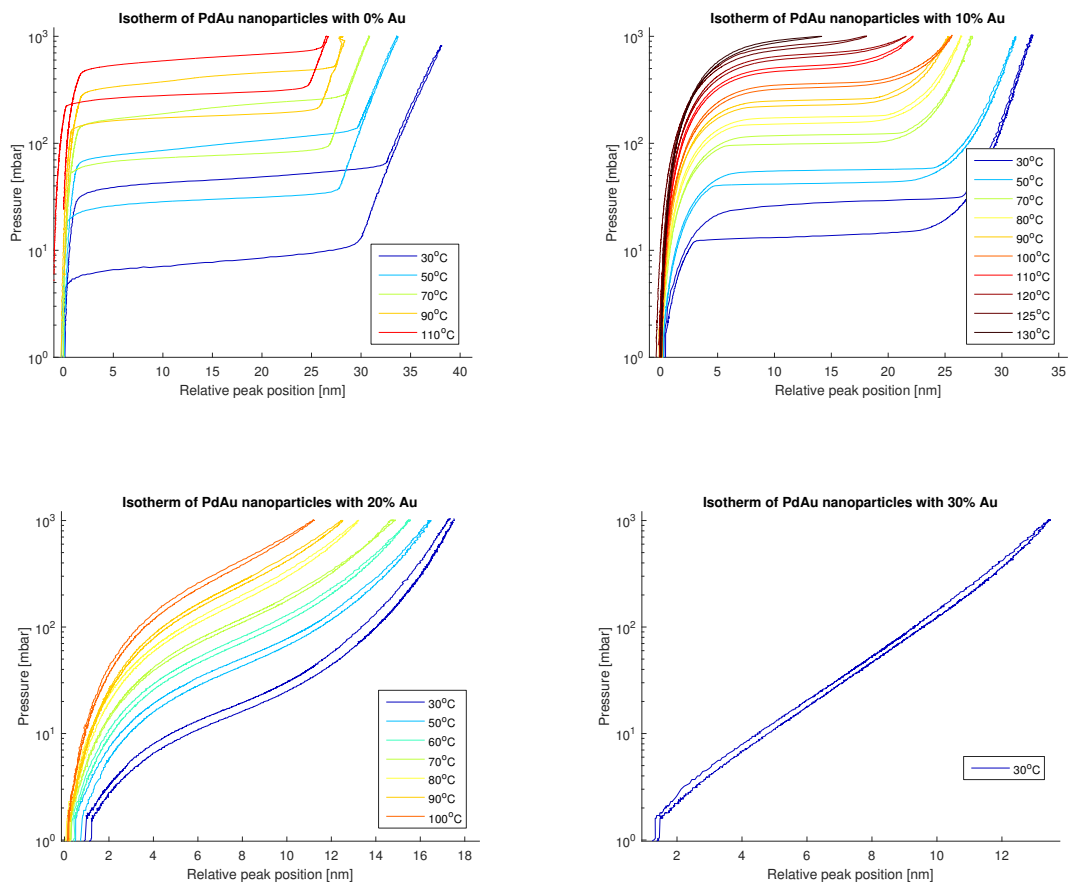


Figure A.2: The figure shows the first measurement series (S1) of isotherms for PdAu nanoparticles with varying amount of gold, 0, 10, 20 and 30%, and at different temperatures, but extracted from peak position instead of extinction. Both ways to interpret the data show the same trends but with slight variation in shape.

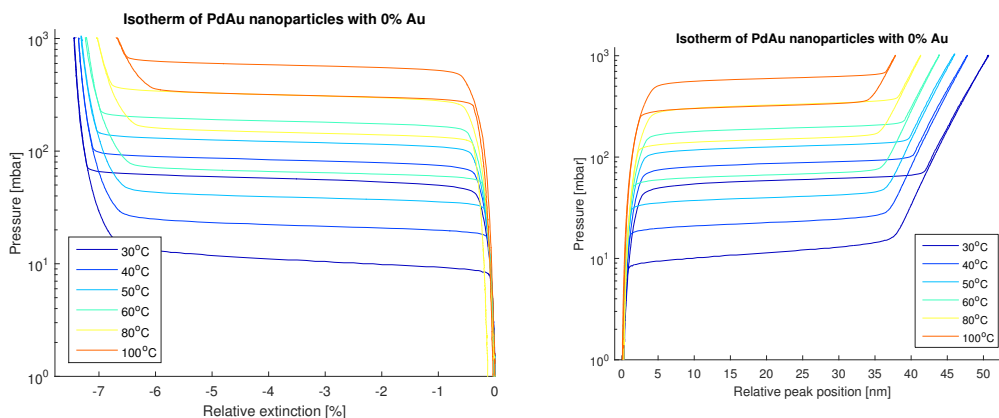


Figure A.3: The figure show isotherms from S2 for 0% gold concentration extracted from extinction at peak position to the left and from peak position to the right. The general shapes are very similar to those of S1 for 0% seen in figure 4.1 and A.2, indicating reproducibility.

A.3 More relations between extinction spectrum descriptors

In this section additional graphs to show the amount of data contained in relating different descriptors are presented. Peak position versus extinction for additional temperatures is shown in figures A.4, A.5, A.6, A.7 and A.8. To show this can also be done for FWHM, graphs of such data extraction are seen in figures A.9, A.10, A.11, A.12, A.13 and A.14. Many more comparisons can be made to get additional information regarding the extinction spectra during hydrogenation. The graphs displayed here at least show the great amount of information stored within measurements with this technique.

These kind of observations has been made before which indicates that the relation between the descriptors is related to the behavior of the extinction spectra and is not a measurement artifact. An example of this is displayed in figure A.15, where this was done for the same type of particles but only annealed for 6 hours. The shorter annealing time results in a more pronounced hysteresis but otherwise the relation between peak position and extinction at peak position is very much the same.

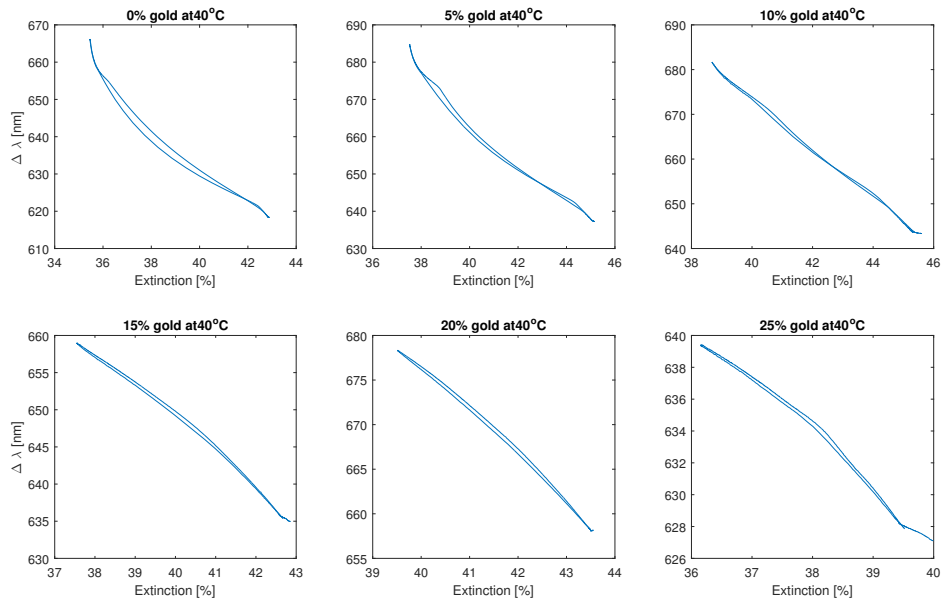


Figure A.4: The graphs compare peak position with the extinction at peak position for the measurements at 40°C presented in figure 4.2.

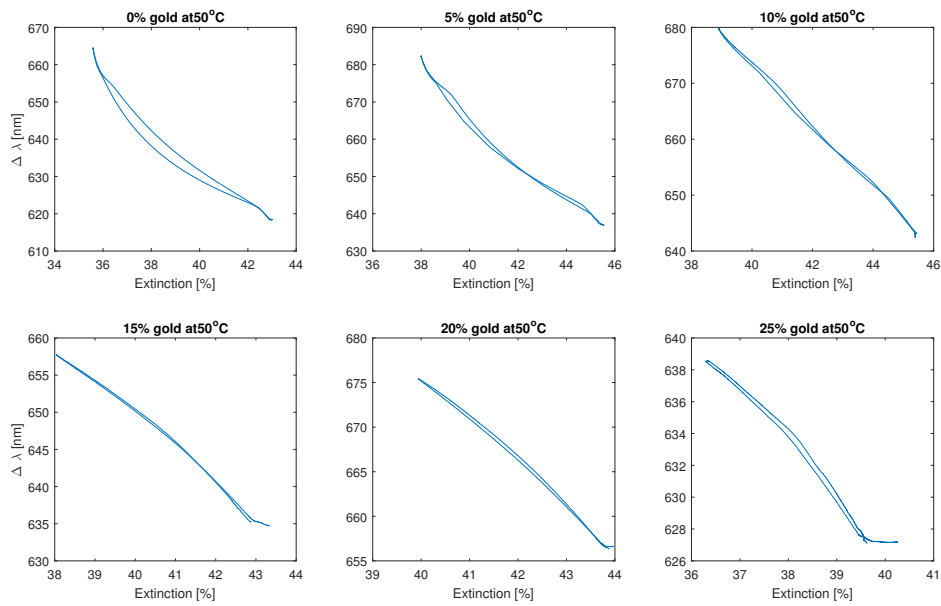


Figure A.5: The graphs compare peak position with the extinction at peak position for the measurements at 50°C presented in figure 4.2.

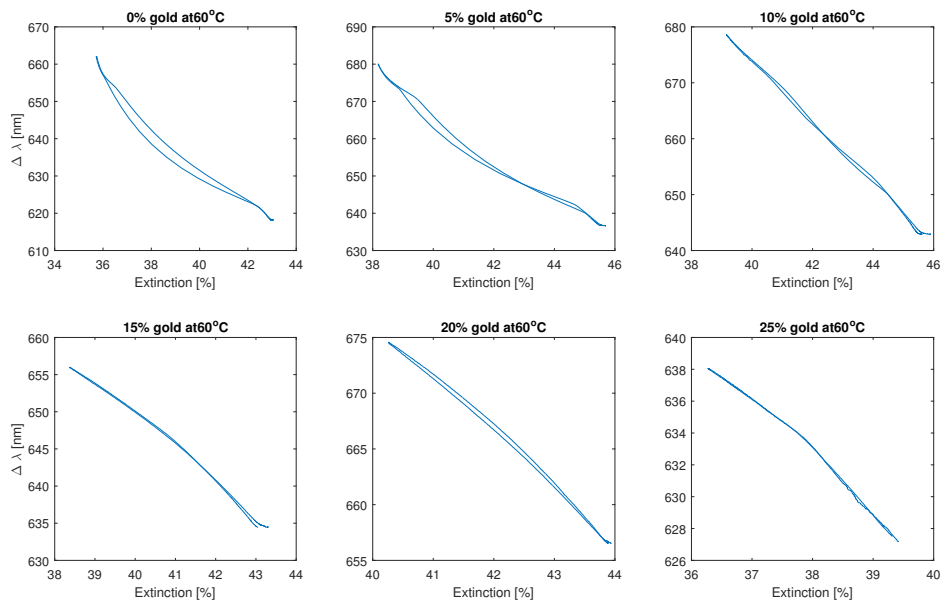


Figure A.6: The graphs compare peak position with the extinction at peak position for the measurements at 60°C presented in figure 4.2.

A. Appendix 1

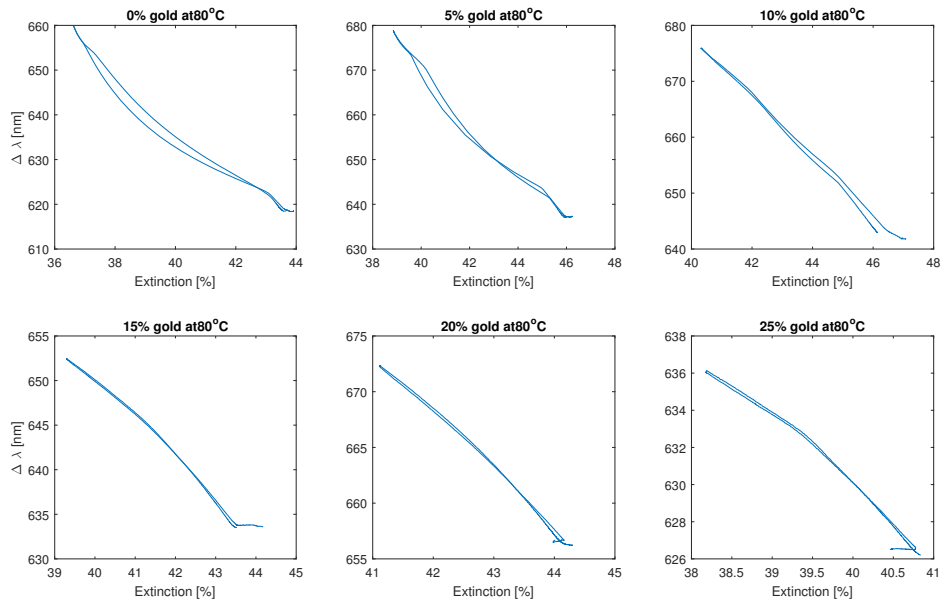


Figure A.7: The graphs compare peak position with the extinction at peak position for the measurements at 80°C presented in figure 4.2.

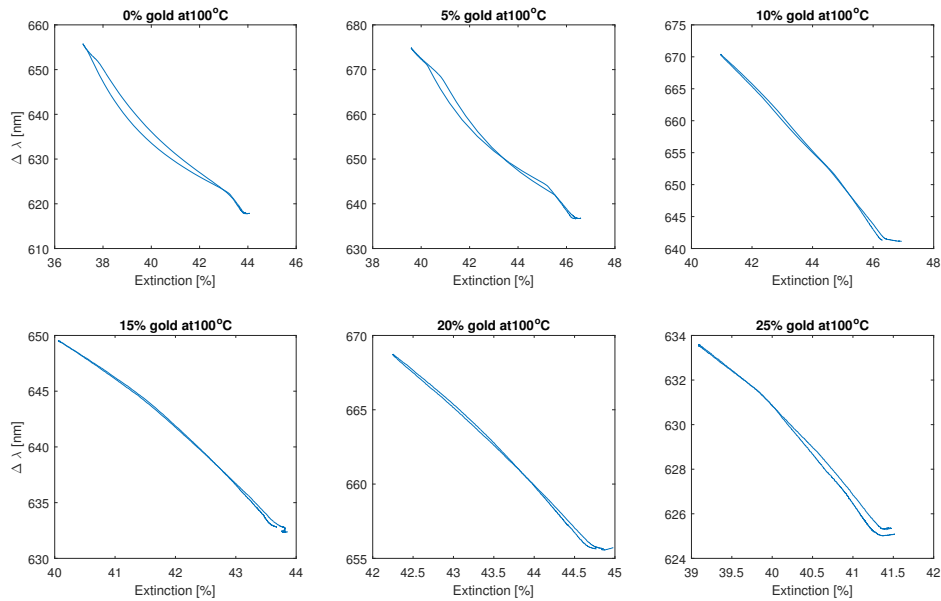


Figure A.8: The graphs compare peak position with the extinction at peak position for the measurements at 100°C presented in figure 4.2.

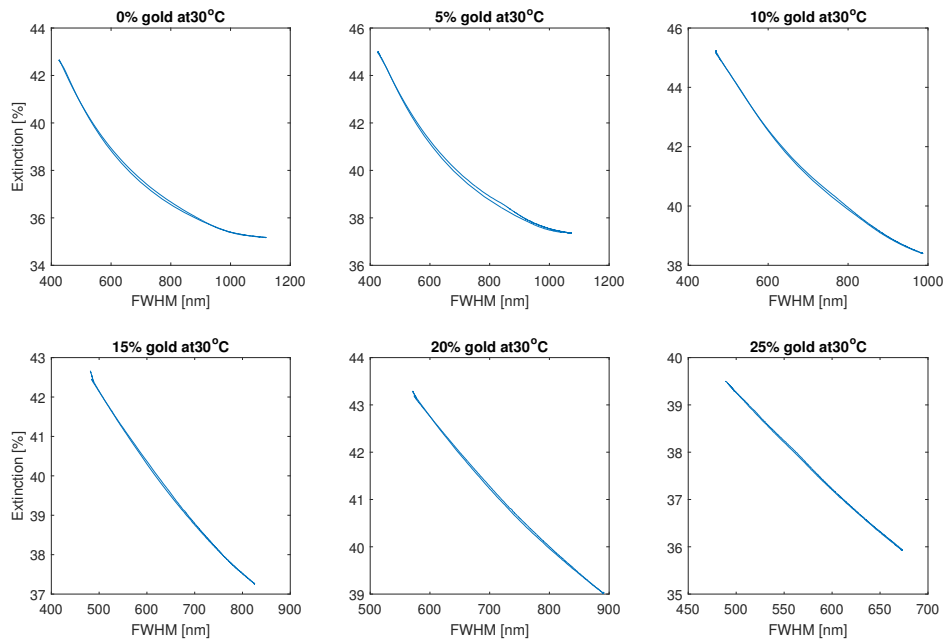


Figure A.9: The graphs compare FWHM with the extinction at peak position for the measurements at 30°C presented in figure 4.2.

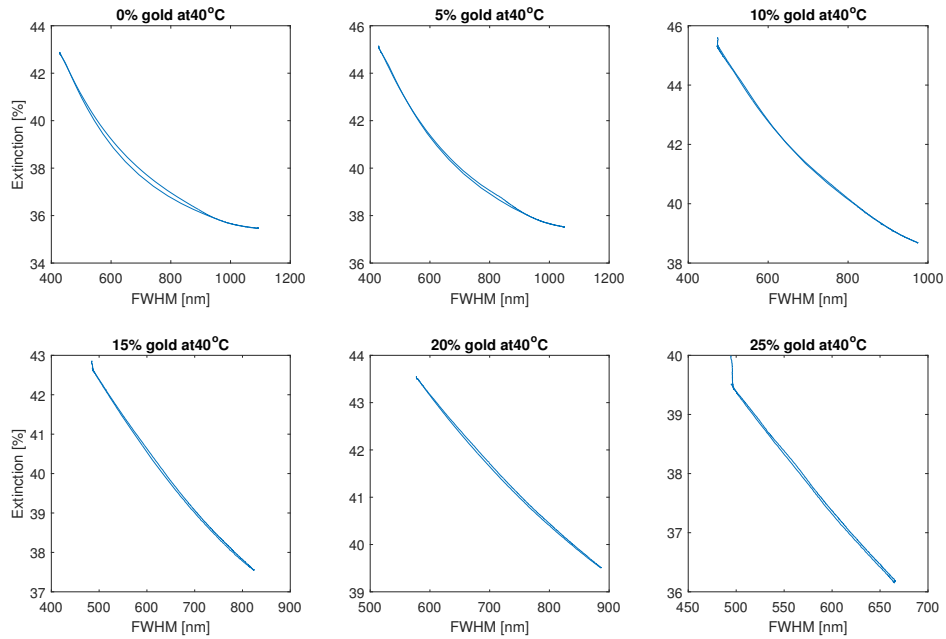


Figure A.10: The graphs compare FWHM with the extinction at peak position for the measurements at 40°C presented in figure 4.2.

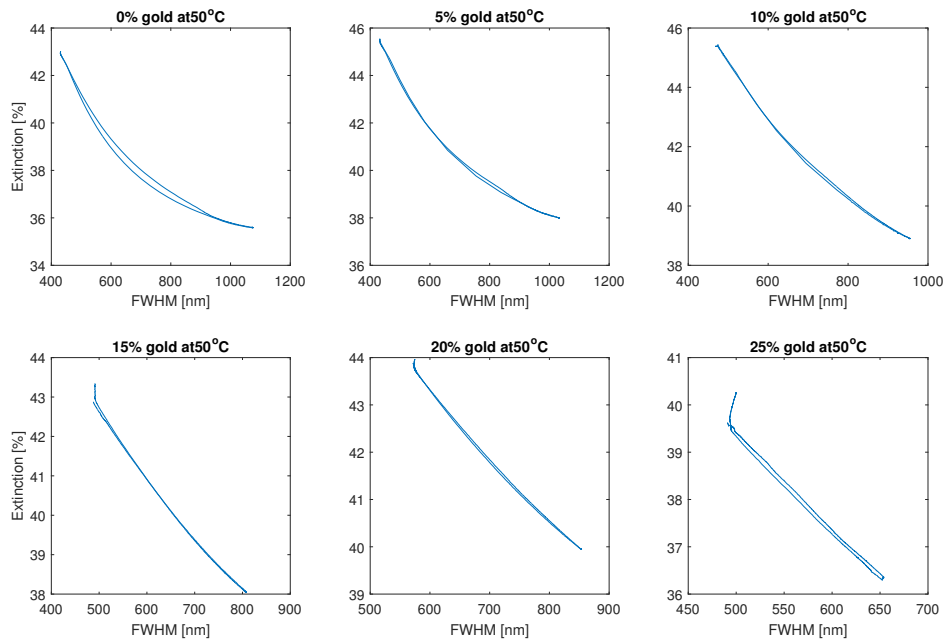


Figure A.11: The graphs compare FWHM with the extinction at peak position for the measurements at 50°C presented in figure 4.2.

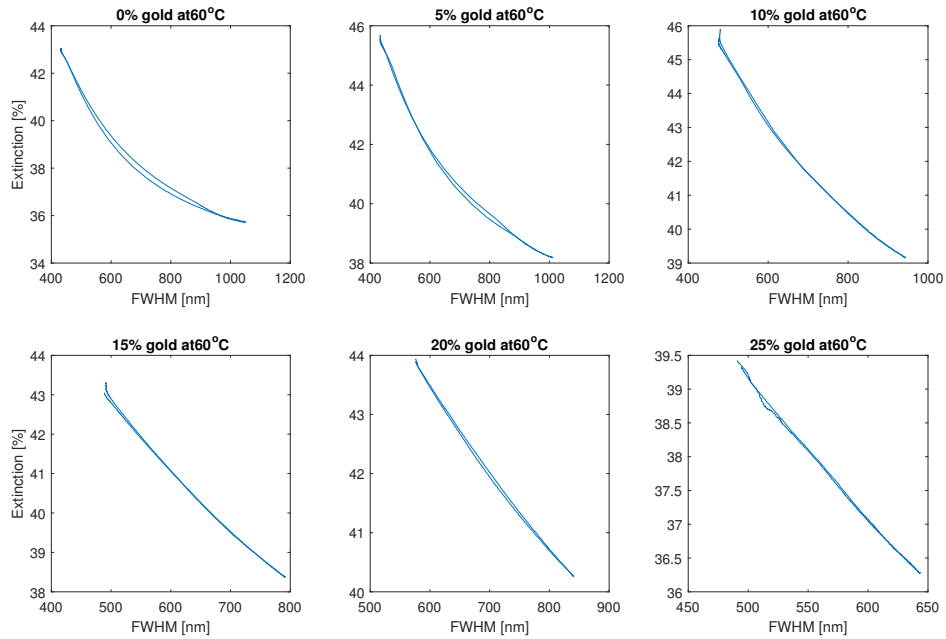


Figure A.12: The graphs compare FWHM with the extinction at peak position for the measurements at 60°C presented in figure 4.2.

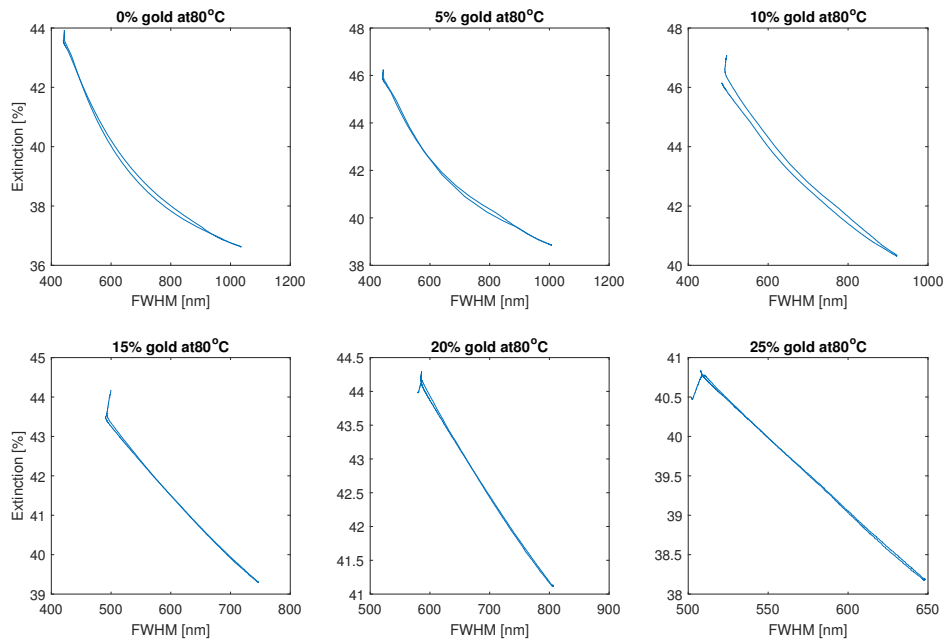


Figure A.13: The graphs compare FWHM with the extinction at peak position for the measurements at 80°C presented in figure 4.2.

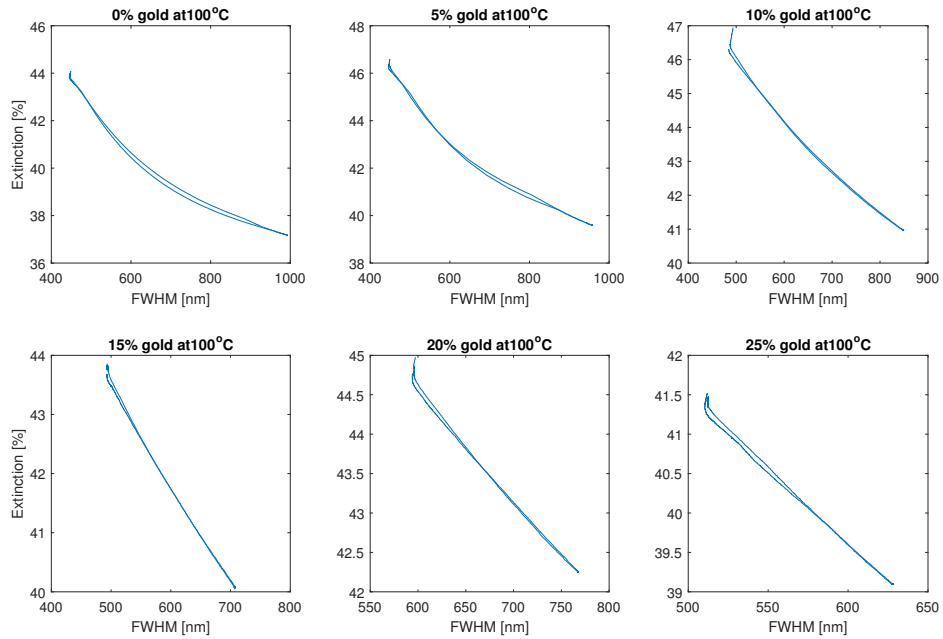


Figure A.14: The graphs compare FWHM with the extinction at peak position for the measurements at 100°C presented in figure 4.2.

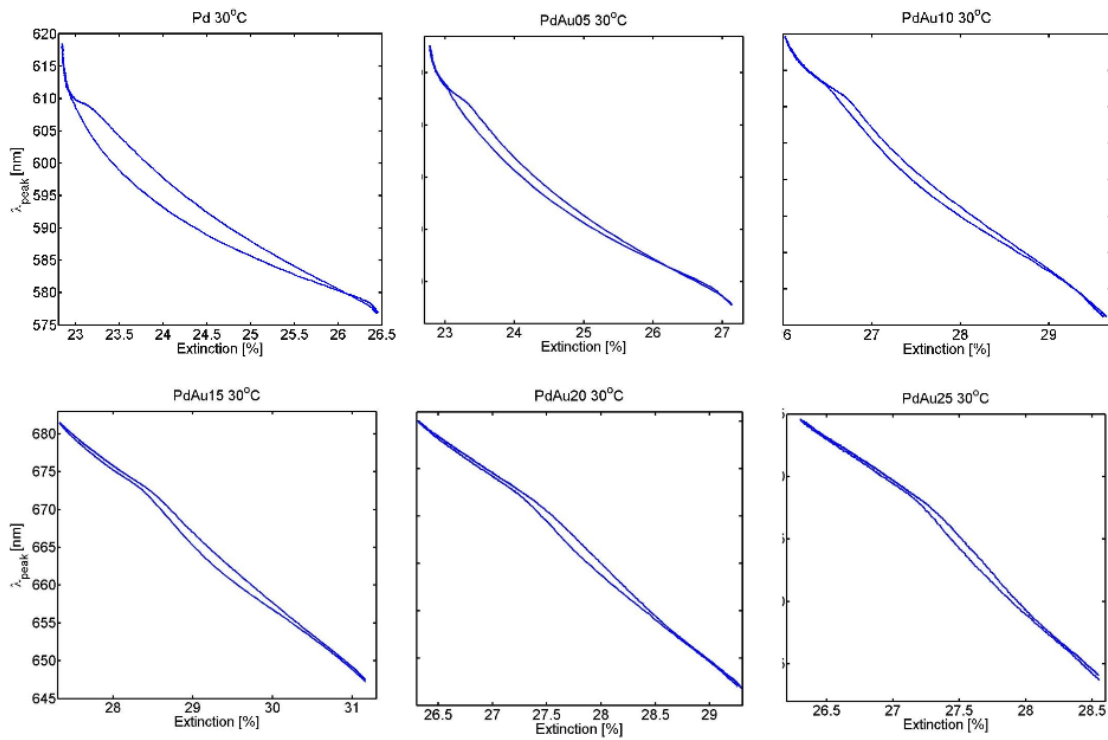


Figure A.15: The graphs compare peak position with the extinction at peak position for the measurements at 30°C done by Ferry Nugroho. We here see very similar trends to the ones in figure 4.10, however with a more pronounced hysteresis due to shorter annealing time.

A.4 Van't Hoff plots

Additional Van't Hoff plots are presented in figures A.16, A.17, A.18, A.19 and A.20. Here figure A.16 is from measurement series S1 while the rest are from S2.

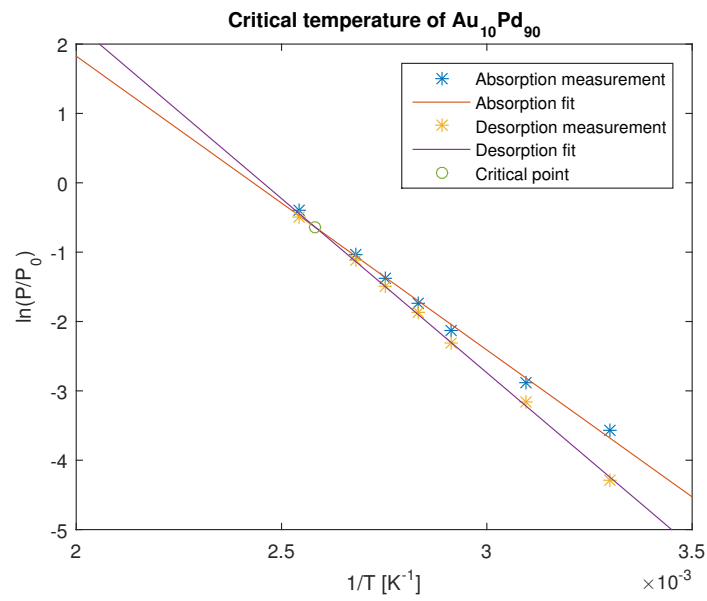


Figure A.16: The graph shows the Van't Hoff plot for evaluating T_C for 10% gold in measurement series S1.

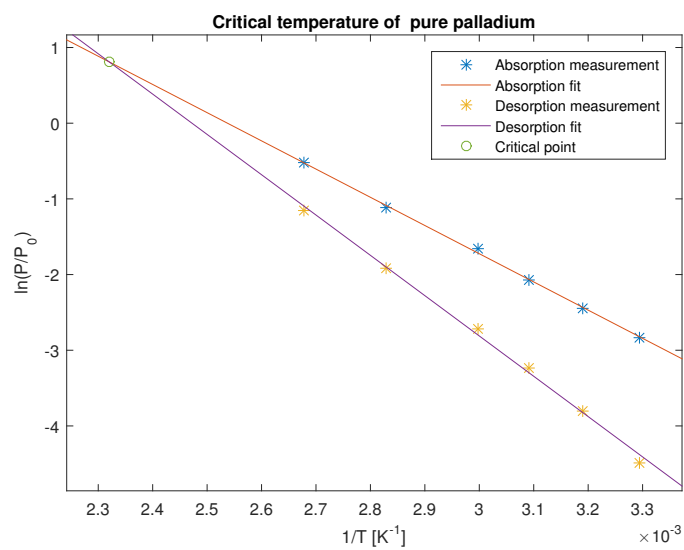


Figure A.17: The graph shows the Van't Hoff plot for evaluating T_C for 0% gold in measurement series S2.

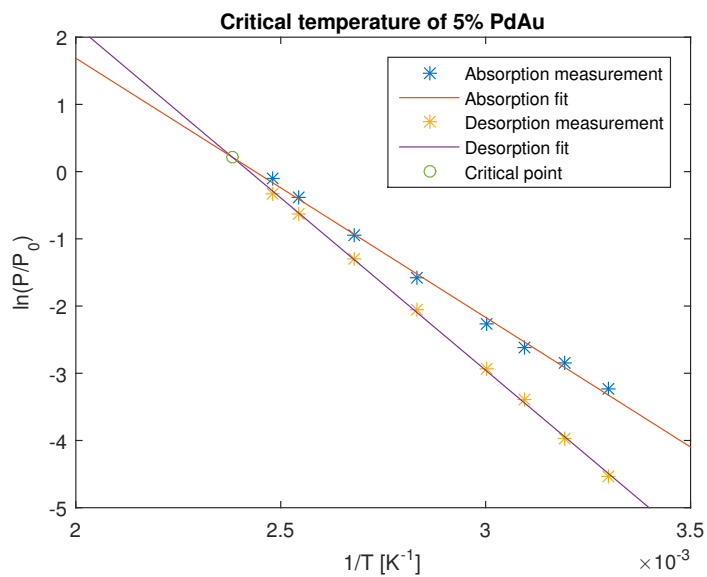


Figure A.18: The graph shows the Van't Hoff plot for evaluating T_C for 5% gold in measurement series S2.

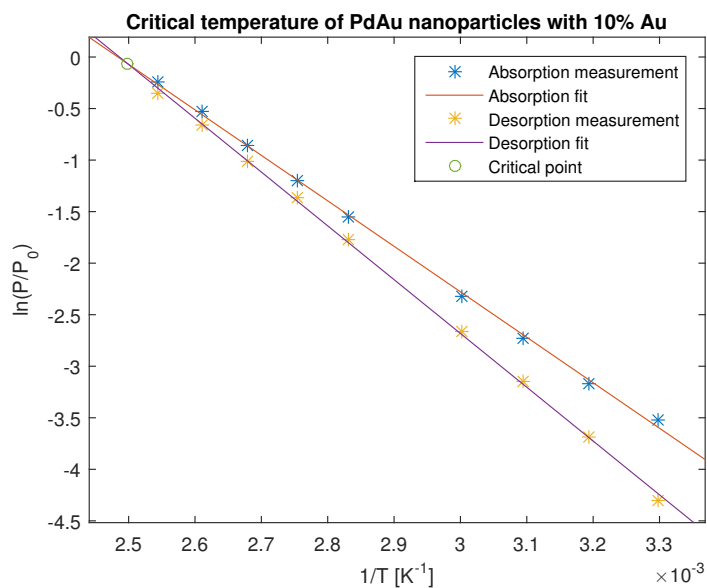


Figure A.19: The graph shows the Van't Hoff plot for evaluating T_C for 10% gold in measurement series S2.

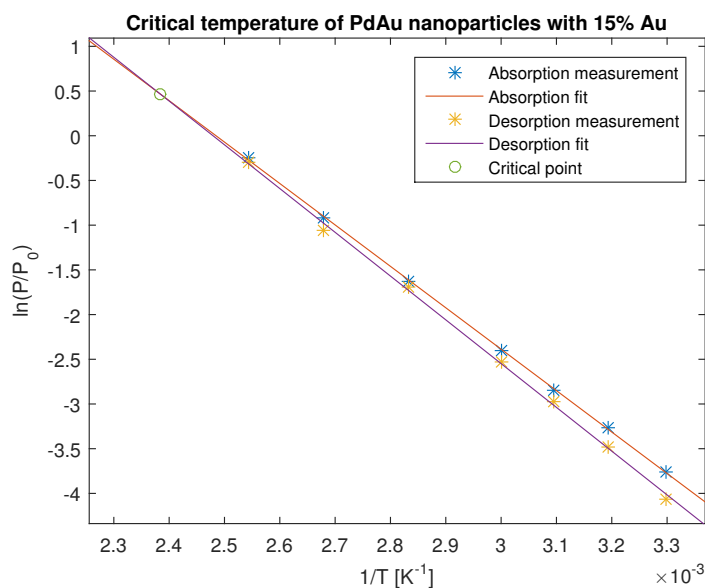


Figure A.20: The graph shows the Van't Hoff plot for evaluating T_C for 15% gold in measurement series S2.

A.5 Data collapse for S1

Data collapse was also performed on measurement series S1 and the result from this is displayed in figure A.21.

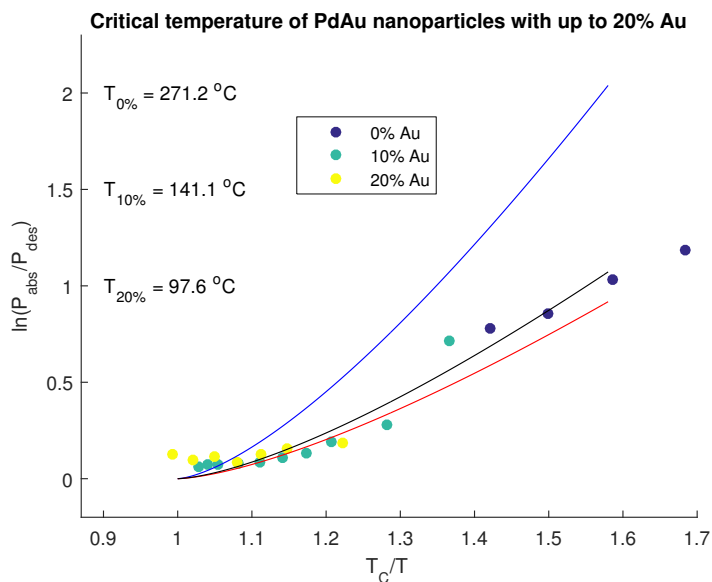


Figure A.21: In this graph data collapse on S1 is shown. The amount of contribution from isotherms with large overall hysteresis gives a fairly low k -factor of 0.526. This contribution most likely results in a slight overestimation of T_C .